

ARTICLE

Received 10 Jul 2016 | Accepted 8 Nov 2016 | Published 19 Dec 2016

DOI: 10.1038/ncomms13879

OPEN

A Mott insulator continuously connected to iron pnictide superconductors

Yu Song¹, Zahra Yamani², Chongde Cao^{1,3}, Yu Li¹, Chenglin Zhang¹, Justin S. Chen¹, Qingzhen Huang⁴, Hui Wu^{4,5}, Jing Tao⁶, Yimei Zhu⁶, Wei Tian⁷, Songxue Chi⁷, Huibo Cao⁷, Yao-Bo Huang^{8,9}, Marcus Dantz⁸, Thorsten Schmitt⁸, Rong Yu^{10,11,12}, Andriy H. Nevidomskyy¹, Emilia Morosan¹, Qimiao Si¹ & Pengcheng Dai¹

Iron-based superconductivity develops near an antiferromagnetic order and out of a bad-metal normal state, which has been interpreted as originating from a proximate Mott transition. Whether an actual Mott insulator can be realized in the phase diagram of the iron pnictides remains an open question. Here we use transport, transmission electron microscopy, X-ray absorption spectroscopy, resonant inelastic X-ray scattering and neutron scattering to demonstrate that $\text{NaFe}_{1-x}\text{Cu}_x\text{As}$ near $x \approx 0.5$ exhibits real space Fe and Cu ordering, and are antiferromagnetic insulators with the insulating behaviour persisting above the Néel temperature, indicative of a Mott insulator. On decreasing x from 0.5, the antiferromagnetic-ordered moment continuously decreases, yielding to superconductivity $\sim x = 0.05$. Our discovery of a Mott-insulating state in $\text{NaFe}_{1-x}\text{Cu}_x\text{As}$ thus makes it the only known Fe-based material, in which superconductivity can be smoothly connected to the Mott-insulating state, highlighting the important role of electron correlations in the high- T_c superconductivity.

¹Department of Physics and Astronomy and Rice Center for Quantum Materials, Rice University, Houston, Texas 77005, USA. ²Canadian Neutron Beam Centre, Chalk River Laboratories, Chalk River, Ontario K0J 1J0, Canada. ³Department of Applied Physics, Northwestern Polytechnical University, Xian 710072, China. ⁴NIST Center for Neutron Research, National Institute of Standards and Technology, Gaithersburg, Maryland 20899, USA. ⁵Department of Materials Science and Engineering, University of Maryland, College Park, Maryland 20742-2115, USA. ⁶Department of Condensed Matter Physics and Materials Science, Brookhaven National Laboratory, Upton, New York 11973, USA. ⁷Quantum Condensed Matter Division, Oak Ridge National Laboratory, Oak Ridge, Tennessee 37831, USA. ⁸Paul Scherrer Institute, Swiss Light Source, CH-5232 Villigen PSI, Switzerland. ⁹Beijing National Laboratory for Condensed Matter Physics, and Institute of Physics, Chinese Academy of Sciences, Beijing 100190, China. ¹⁰Department of Physics and Beijing Key Laboratory of Opto-electronic Functional Materials & Micro-nano Devices, Renmin University of China, Beijing 100872, China. ¹¹Department of Physics and Astronomy, Shanghai Jiao Tong University, Shanghai 200240, China. ¹²Collaborative Innovation Center of Advanced Microstructures, Nanjing 210093, China. Correspondence and requests for materials should be addressed to Q.S. (email: qmsi@rice.edu) or to P.D. (email: pdai@rice.edu).

At the heart of understanding the physics of the iron-based superconductors is the interplay of superconductivity, magnetism and bad-metal behaviour^{1–6}. A key question is whether superconductivity emerges due to strong electronic correlations^{6–11} or nested Fermi surfaces^{12–14}. Superconductivity occurs in the vicinity of antiferromagnetic (AF) order, both in the iron pnictides and iron chalcogenides^{2–5}. In addition, the normal state has a very large room temperature resistivity, which reaches the Ioffe–Mott–Regel limit^{2,4,5}. This bad-metal behaviour has been attributed to the proximity to a Mott transition^{7–11}, with the Coulomb repulsion of the multi-orbital $3d$ electrons of the Fe ions being close to the threshold for electronic localization. In the iron chalcogenide family, several compounds have been found to be AF and insulating with characteristic features of a Mott insulator^{15–18}. There is also evidence for an orbital-selective Mott phase in $A_x\text{Fe}_{2-y}\text{Se}_2$ ($A = \text{K}, \text{Rb}$)¹⁹. However, in these iron chalcogenide materials, one cannot continuously tune the AF Mott-insulating state into a superconductor. On the other hand, the iron pnictide $\text{NaFe}_{1-x}\text{Cu}_x\text{As}$ is a plausible candidate for a Mott insulator based on transport and scanning tunnelling microscopy (STM) measurements near $x = 0.3$ (refs 20,21); however, the insulating behaviour may also be induced by Anderson localization via Cu-disorder.

The parent compounds of iron pnictide superconductors such as AFe_2As_2 ($A = \text{Ba}, \text{Sr}, \text{Ca}$) and NaFeAs have crystal structures shown in Fig. 1a,b, respectively². They exhibit a tetragonal-to-orthorhombic structural phase transition at temperature T_s , followed by a paramagnetic to AF phase transition at T_N ($T_s \geq T_N$) with a collinear magnetic structure, where the spins are aligned antiferromagnetically along the a axis of the orthorhombic lattice (Fig. 1c)^{22,23}. When Fe in AFe_2As_2 is replaced by Cu to form ACu_2As_2 (ref. 24), the Cu atoms have a nonmagnetic $3d^{10}$ electronic configuration with Cu^{1+} and a filled d shell due to the presence of a covalent bond between the As atoms within the same unit cell $[\text{As}]^{-3} \equiv [\text{As}-\text{As}]^{-4/2}$ shown as the shaded As–As bond in Fig. 1a^{25–28}, as predicted by band structure calculations²⁹. Since the crystal structure of $\text{NaFe}_{1-x}\text{Cu}_x\text{As}$ does not allow a similar covalent bond (Fig. 1b)²⁰, it would be interesting to explore the magnetic state of $\text{NaFe}_{1-x}\text{Cu}_x\text{As}$ in the heavily Cu-doped regime. From transport measurements on single crystals of $\text{NaFe}_{1-x}\text{Cu}_x\text{As}$ with $x \leq 0.3$, it was found that the in-plane resistivity of the system becomes insulating-like for $x \geq 0.11$ (ref. 20). STM showed that local density of states for $\text{NaFe}_{1-x}\text{Cu}_x\text{As}$ with $x = 0.3$ resembles electron-doped Mott insulators²¹, although it is unclear what the undoped Mott-insulating state is or whether it exhibits AF order.

Using transport, neutron scattering, transmission electron microscopy (TEM), X-ray absorption spectroscopy (XAS) and resonant inelastic X-ray scattering (RIXS), we demonstrate that heavily Cu-doped $\text{NaFe}_{1-x}\text{Cu}_x\text{As}$ exhibits Fe and Cu ordering, and becomes an AF insulator when x approaches 0.5. The insulating behaviour persists into the paramagnetic state, providing strong evidence for a Mott-insulating state. This conclusion is corroborated by our theoretical calculations based on the $U(1)$ slave-spin approach³⁰. Our calculations demonstrate enhanced correlations and a Mott localization from the combined effect of a bandwidth reduction, which results from a Cu-site blockage of the kinetic motion of the Fe $3d$ electrons, and a hole doping from $3d^6$ to $3d^5$, both of which are made possible by the fully occupied Cu $3d$ shell^{7,9–11,30}. On decreasing x from $x \approx 0.5$, the correlation lengths of Fe and Cu ordering, and magnetic ordering, as well as the ordered magnetic moment continuously decrease, connecting smoothly with the superconducting phase in $\text{NaFe}_{1-x}\text{Cu}_x\text{As}$ appearing near

$x = 0.05$, highlighting the role of electronic correlations in iron pnictides.

Results

Resistivity measurements. Single crystals of $\text{NaFe}_{1-x}\text{Cu}_x\text{As}$ were prepared using the self-flux method. Transport measurements were carried out using a commercial physical property measurement system with the standard four-probe method (the Methods section). Figure 1e shows temperature dependence of the in-plane resistivity for the $x = 0.016$ sample. In addition to superconductivity at $T_c = 11$ K, the normal state resistivity ρ is ~ 0.4 m Ω cm at room temperature, consistent with previous work²⁰. Figure 1f plots the temperature dependence of the resistivity on a log scale for samples with $x = 0.18, 0.38, 0.44$ and 0.48 . Resistivity in the $x = 0.18$ sample exhibits insulating-like behaviour consistent with earlier work²⁰. For the $x \geq 0.39$ samples, resistivity further increases by an order of magnitude compared to the $x = 0.18$ sample, signifying that electrons become much more localized in $\text{NaFe}_{1-x}\text{Cu}_x\text{As}$, when x approaches 0.5.

Neutron scattering results on $\text{NaFe}_{0.56}\text{Cu}_{0.44}\text{As}$. Unpolarized and polarized elastic neutron scattering were carried out on $\text{NaFe}_{1-x}\text{Cu}_x\text{As}$ single-crystal samples (the Methods section). For these measurements, we use the orthorhombic unit cell notation suitable for the AF-ordered state of NaFeAs (refs 22,23), and define momentum transfer \mathbf{Q} in three-dimensional reciprocal space in \AA^{-1} as $\mathbf{Q} = H\mathbf{a}^* + K\mathbf{b}^* + L\mathbf{c}^*$, where H, K and L are Miller indices and $\mathbf{a}^* = \hat{\mathbf{a}}2\pi/a$, $\mathbf{b}^* = \hat{\mathbf{b}}2\pi/b$ and $\mathbf{c}^* = \hat{\mathbf{c}}2\pi/c$ (Fig. 1c). Single crystals are aligned in the $(H, 0, L)$ and (H, H, L) scattering planes in these measurements. In the $(H, 0, L)$ scattering geometry, the collinear magnetic structure in NaFeAs (Fig. 1c) gives magnetic Bragg peaks below T_N at $\mathbf{Q}_{\text{AF}} = (H, 0, L)$, where $H = 1, 3, \dots$ and $L = 0.5, 1.5, \dots$, positions^{22,23}.

Figure 2c shows typical elastic scans for $\text{NaFe}_{0.56}\text{Cu}_{0.44}\text{As}$ along the $[H, 0, 0.5]$ direction at $T = 3.6$ and 300 K. Because of twinning in the orthorhombic state, this is equivalent to elastic scans along the $[0, K, 0.5]$ direction. While the scattering has a clear peak centred around $\mathbf{Q} = (1, 0, 0.5)/(0, 1, 0.5)$ at room temperature, the scattering is enhanced markedly on cooling to 3.6 K, suggesting the presence of static AF order. The temperature difference plot between 3.6 and 300 K in Fig. 2d indicates that the low-temperature intensity gain is essentially instrumental resolution limited (horizontal bar). Figure 2e shows the temperature difference along the $[1, 0, L]/[0, 1, L]$ direction that apparently is not resolution limited. The temperature dependence of the scattering at $(1, 0, 0.5)/(0, 1, 0.5)$ plotted in Fig. 2f reveals clear evidence of magnetic ordering below $T_N \approx 200$ K, suggesting that the small peak observed at room temperature in Fig. 2c occurs in the paramagnetic phase and is thus of structural (super-lattice) origin induced by Cu substitution, since such a peak is forbidden for NaFeAs .

Fe and Cu ordering in $\text{NaFe}_{1-x}\text{Cu}_x$ with $x \approx 0.5$. To conclusively determine the origin of super-lattice peaks and the crystal structure of $\text{NaFe}_{0.56}\text{Cu}_{0.44}\text{As}$, we have carried out high-resolution TEM measurements. The inset in Fig. 2a shows an image of the sample, and the electron diffraction patterns were collected from areas ~ 100 nm in diameter within a single domain of the sample (see the arrow in the inset of Fig. 2a). A typical diffraction pattern along the $[001]$ zone axis at room temperature is shown in Fig. 2a. While we see clear super-lattice reflections at $H = 1, 3, \dots$ positions along the $[H, 0, 0]$ direction,

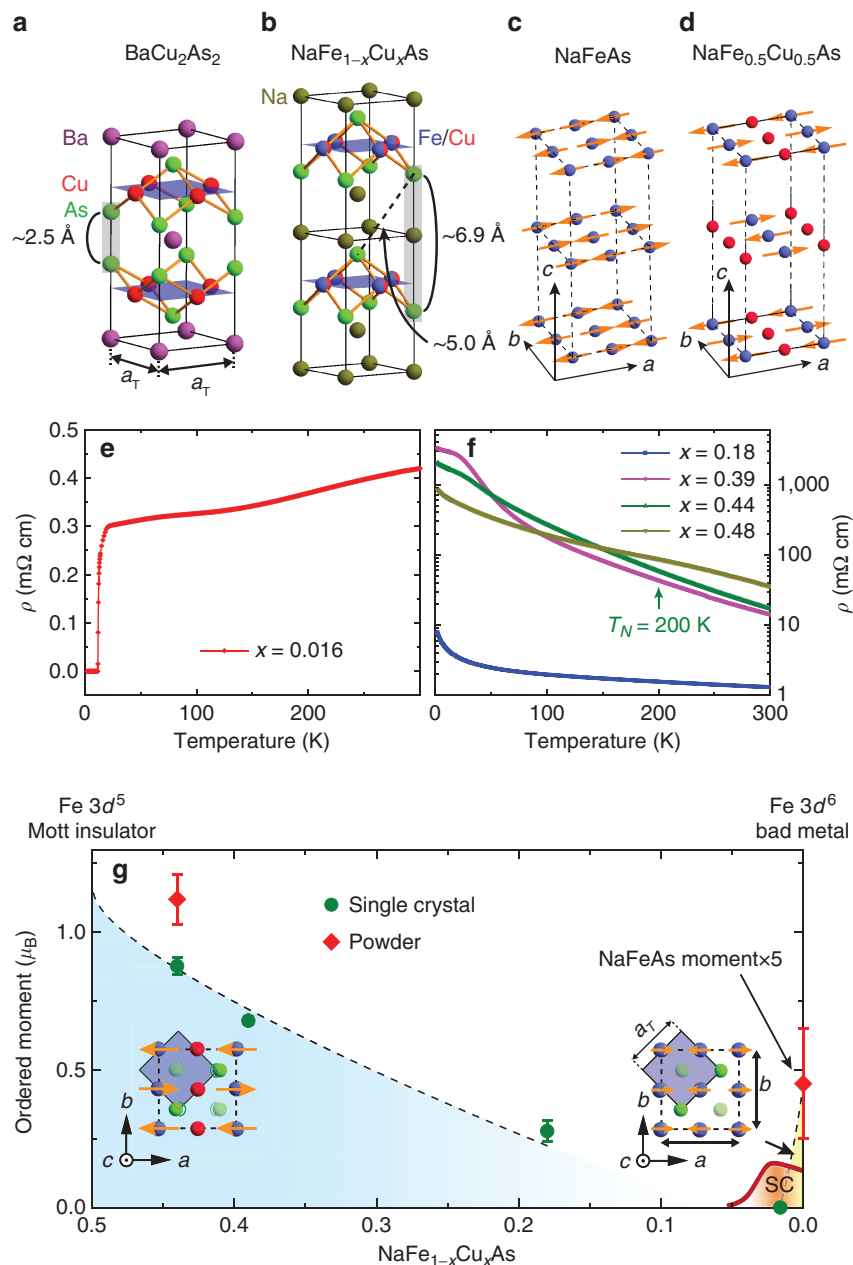


Figure 1 | Summary of transport and neutron scattering results. (a) The crystal structure of ACu_2As_2 in the tetragonal state, where a_T is the in-plane lattice parameter. The As-As covalent bonding distance is ~ 2.5 Å. (b) The crystal structure of $NaFe_{1-x}Cu_xAs$, where similar As-As covalent bonding is not possible. (c) The collinear magnetic structure of $NaFeAs$, where the AF order and moment direction are along the orthorhombic a axis^{22,23}. Only Fe atoms are plotted in the figure for clarity. (d) Real space structure and spin arrangements of $NaFe_{0.5}Cu_{0.5}As$ in the AF orthorhombic unit cell similar to $NaFeAs$. In $NaFe_{0.5}Cu_{0.5}As$, since Fe and Cu form stripes, Na and As also shift slightly from their high-symmetry positions. (e) In-plane resistivity for $x = 0.016$ sample, where bulk superconductivity occurs below $T_c = 11$ K (ref. 20). (f) Temperature dependence of the in-plane resistivity for $x = 0.18, 0.39, 0.44$ and 0.48 samples. The vertical arrow marks the position of T_N for the $x = 0.44$ sample determined from neutron scattering. (g) Evolution of ordered moment with doping in $NaFe_{1-x}Cu_xAs$. The two ordered phases are separated by the superconducting dome marked as SC, with no magnetic order for $x = 0.016$ near optimal superconductivity. The right and left insets show the in-plane magnetic structures of $NaFeAs$ and the new AF insulating phase, respectively. For $x \leq 0.05$, the phase diagram from ref. 20 is plotted. Vertical error bars are from least-square fits (1 s.d.).

they are absent at the $K = 1, 3, \dots$ positions along the $[0, K, 0]$ direction (Fig. 2b). This means that the crystal structure of $NaFe_{0.56}Cu_{0.44}As$ is orthorhombic and obeys two-fold rotational symmetry. From this information and from intensities of the super-lattice peaks in $(H, 0, L)$ scattering plane, we conclude that Fe and Cu atoms in $NaFe_{0.5}Cu_{0.5}As$ (which is approximated by $NaFe_{0.56}Cu_{0.44}As$) form a real space stripe-like-ordered structure in Fig. 1d, in the space group $Ibam$ (Supplementary Note 1;

Supplementary Table 1). This conclusion is further corroborated by single-crystal neutron diffraction measurements (Supplementary Table 2). The Fe-Cu ordering is a structural analogue of the magnetic order in $NaFeAs$ and structural super-lattice peaks occur at the same positions as magnetic peaks in $NaFeAs$. Fe and Cu ordering in $NaFe_{1-x}Cu_xAs$ affects the intensities of Bragg peaks already present in $NaFeAs$ very little (Supplementary Note 1; Supplementary Fig. 1), and the induced

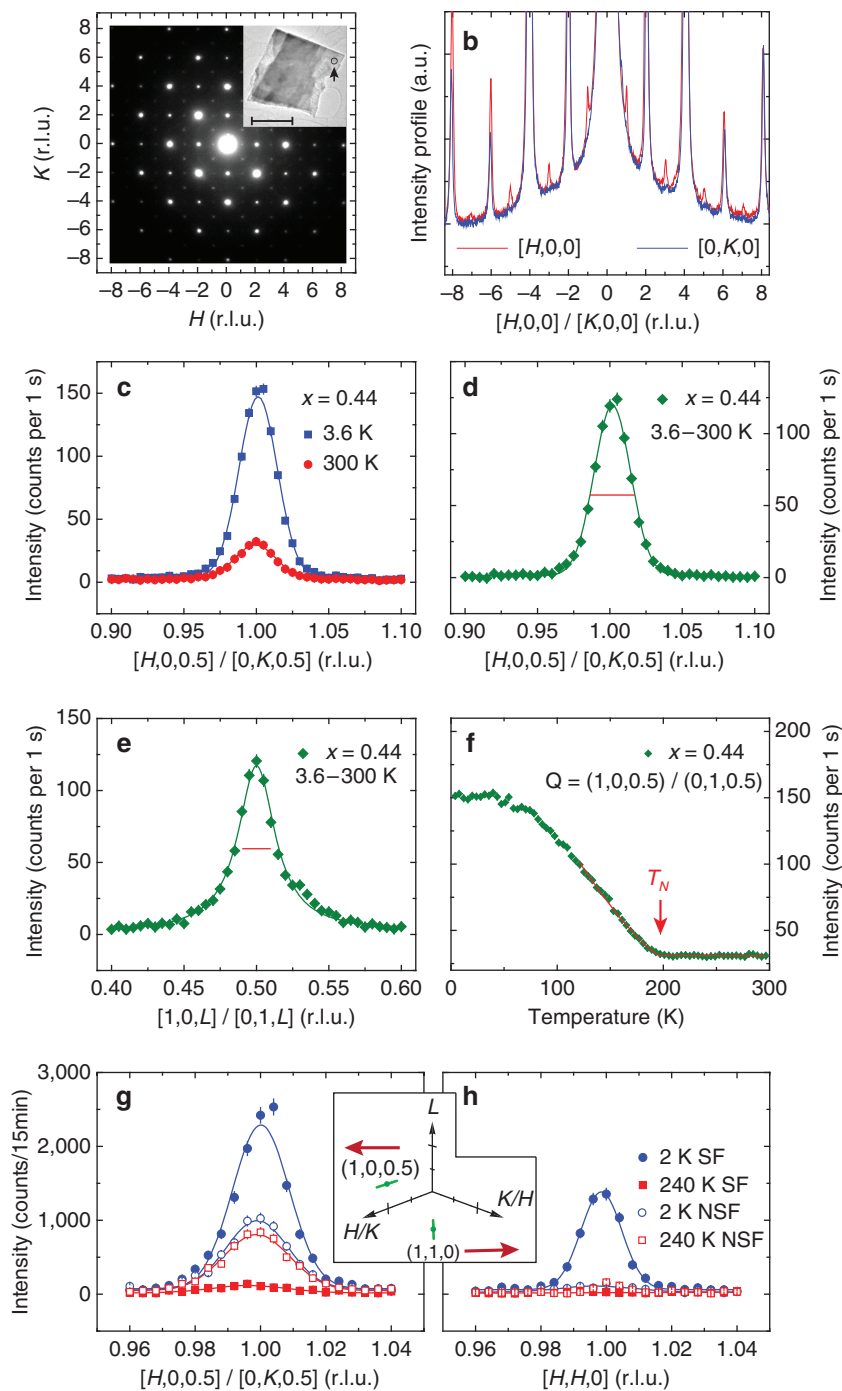


Figure 2 | TEM and neutron scattering results on the structure and magnetic order for $\text{NaFe}_{0.56}\text{Cu}_{0.44}\text{As}$. (a) Using 200 keV incident electrons, an electron diffraction pattern in the $[H, K]$ plane was obtained from a $\text{NaFe}_{0.56}\text{Cu}_{0.44}\text{As}$ particle with its TEM real space image shown in the inset. Scale bar, is $1\ \mu\text{m}$. (b) Cuts of **a** along the $[H, 0]$ and $[0, K]$ directions. (c) Unpolarized neutron diffraction scans along the $[H, 0, 0.5]/[0, K, 0.5]$ direction for the $x = 0.44$ sample at 300 and 3.6 K. The peak at 300 K is a super-lattice peak arising from Fe–Cu ordering. Temperature difference plots between 3.6 and 300 K along the (d) $[H, 0, 0.5]/[0, K, 0.5]$ and (e) $[1, 0, L]/[0, 1, L]$ directions. Solid lines are Gaussian fits and the horizontal bars indicate instrumental resolution. (f) Temperature dependence of the scattering at $\mathbf{Q} = (1, 0, 0.5)/(0, 1, 0.5)$ shows $T_N \approx 200\ \text{K}$. (g) Neutron polarization analysis of the magnetic Bragg peak at $(1, 0, 0.5)/(0, 1, 0.5)$. Neutron SF and NSF cross-sections are measured at 2 and 240 K. The peak at 240 K is nonmagnetic nuclear scattering giving rise to NSF scattering. (h) Similar scans for the $(1, 1, 0)$ peak. The inset shows positions of these two peaks in reciprocal space. All vertical error bars represent statistical error (1 s.d.).

super lattice are relatively weak. Aside from ordering of Fe and Cu, other aspects of the structure of $\text{NaFe}_{1-x}\text{Cu}_x\text{As}$ remain identical to that of NaFeAs , corroborated by the similar neutron powder diffraction patterns (Supplementary Note 1; Supplementary Fig. 2; Supplementary Table 3).

Magnetic structure of $\text{NaFe}_{1-x}\text{Cu}_x\text{As}$ with $x \approx 0.5$. Having established the real space Cu and Fe ordering and crystal structure of $\text{NaFe}_{0.56}\text{Cu}_{0.44}\text{As}$, it is important to determine the magnetic states of Cu and Fe. Assuming that the covalent As–As bonding is not possible because of the large distance between the

neighbouring As ions (Fig. 1b), As ions in $\text{NaFe}_{1-x}\text{Cu}_x\text{As}$ can only be in the As^{3-} state. From XAS and RIXS experiments on $\text{NaFe}_{0.56}\text{Cu}_{0.44}\text{As}$ (Supplementary Note 2; Supplementary Fig. 3), we conclude that Cu in $\text{NaFe}_{1-x}\text{Cu}_x\text{As}$ is in the nonmagnetic Cu^{1+} configuration. As a consequence, Fe should be in the $\text{Fe}^{3+} 3d^5$ state, since Na can only be in the Na^{1+} state.

Assuming Fe in $\text{NaFe}_{0.56}\text{Cu}_{0.44}\text{As}$ is indeed in the $\text{Fe}^{3+} 3d^5$ state, we can determine the magnetic structure of the system by systematically measuring magnetic peaks at different wave vectors (Supplementary Note 3; Supplementary Figs 4 and 5) and using neutron polarization analysis (Supplementary Note 3; Supplementary Fig. 6). By polarizing neutrons along the direction of the momentum transfer \mathbf{Q} , neutron spin-flip (SF) scattering is sensitive to the magnetic components perpendicular to \mathbf{Q} , whereas the non-SF (NSF) scattering probes pure nuclear scattering^{31,32}. Figure 2g shows SF and NSF scans along the $[H, 0, 0.5]/[0, K, 0.5]$ direction at $T=2$ and 240 K. Inspection of the data reveals clear magnetic scattering at 2 K that disappears at 240 K, in addition to the temperature-independent NSF nuclear super-lattice reflection. Figure 2h shows the SF and NSF scans along the $[H, H, 0]$ direction at 2 and 240 K. While the SF scattering shows a clear peak at 2 K that disappears on warming to 240 K, the NSF scattering shows no evidence of the super-lattice peaks. From these results and from systematic determination of magnetic and super-lattice scattering intensity at different wave vectors, we conclude that $\text{NaFe}_{0.56}\text{Cu}_{0.44}\text{As}$ forms a collinear magnetic structure with moments aligned along the a axis as shown in the right inset in Fig. 1g. The ordered magnetic moment is $1.12 \pm 0.09 \mu_B/\text{Fe}$ at 4 K determined from neutron powder diffraction (Supplementary Fig. 2e). For this magnetic structure, magnetic peaks are expected and observed at $(0, 1, 0.5)$ and $(1, 1, 0)$ as shown in Fig. 2g,h (Supplementary Fig. 7). The magnetic peaks at $(0, 1, 0.5)$ overlap with super-lattice peaks at $(1, 0, 0.5)$ due to twinning.

Doping dependence of magnetic order in $\text{NaFe}_{1-x}\text{Cu}_x\text{As}$. To determine the Cu-doping dependence of the $\text{NaFe}_{1-x}\text{Cu}_x\text{As}$ -phase diagram, we carried out additional measurements on single crystals of $\text{NaFe}_{1-x}\text{Cu}_x\text{As}$ with $x=0.18$ and 0.39. Figure 3a,b compare the wave vector scans along the $[H, 0, 0.5]/[0, K, 0.5]$ and $[1, 0, L]/[0, 1, L]$ directions for $x=0.18, 0.39$ and 0.44. In each case, the scattering intensity is normalized to the $(2, 0, 0)$ nuclear Bragg peak. With increasing Cu doping, the scattering profile becomes narrower and stronger, changing from a broad peak indicative of the short-range magnetic order in $x=0.18$ and 0.39 to an essentially instrument resolution limited peak with long-range magnetic order at $x=0.44$. Figure 3c shows the doping evolution of the spin-spin correlation length ξ in $\text{NaFe}_{1-x}\text{Cu}_x\text{As}$, suggesting that the increasing spin correlations in $\text{NaFe}_{1-x}\text{Cu}_x\text{As}$ are related to the increasing Cu doping and the concomitant increase in correlation length of Fe and Cu ordering (Supplementary Note 3; Supplementary Fig. 5f). The evolution of the temperature dependent magnetic order parameter with Cu doping is shown in Fig. 3d. For x well < 0.5 , the magnetic transition is gradual and spin-glass-like. However, with x approaching 0.5, the transition at T_N becomes more well defined. In the undoped state, NaFeAs has a small ordered moment of $0.17 \pm 0.03 \mu_B/\text{Fe}$ (ref. 23). On small Cu doping, superconductivity is induced at $x=0.02$ and the static AF order is suppressed²⁰. With further Cu doping, the system becomes an AF insulator, where the ordered moment reaches $\sim 1.1 \mu_B/\text{Fe}$ at $x=0.44$ (the ordered moment per Fe site was determined in the structure for $\text{NaFe}_{0.5}\text{Cu}_{0.5}\text{As}$ (Fig. 1d)). Since the iron moment in $\text{NaFe}_{1-x}\text{Cu}_x\text{As}$ increases with increasing Cu doping, our determined moment is therefore a lower bound for

the ordered moment for Fe in the ideal $\text{NaFe}_{0.5}\text{Cu}_{0.5}\text{As}$, which for $\text{Fe} 3d^5$ can be in either $S=3/2$ or $S=5/2$ spin state.

Discussion

The behaviour in $\text{NaFe}_{1-x}\text{Cu}_x\text{As}$ is entirely different from the bipartite magnetic parent phases seen in the iron oxypnictide superconductor $\text{LaFeAsO}_{1-x}\text{H}_x$, where magnetic parent phases on both sides of the superconducting dome are metallic antiferromagnets³³. In Cu-doped $\text{Fe}_{1-x}\text{Cu}_x\text{Se}$, a metal-insulator transition has been observed $\sim 4\%$ Cu doping, and a localized moment with spin glass behaviour is found near $x \approx 0.12$ (refs 34,35). Although the density functional theory (DFT) calculations suggest that Cu occurs in the $3d^{10}$ configuration and the metal-insulator transition is by a disorder induced Anderson localization in $\text{Fe}_{1-x}\text{Cu}_x\text{Se}$ (ref. 36), the 20–30% solubility limit of the system³⁴ means it is unclear whether $\text{Fe}_{1-x}\text{Cu}_x\text{Se}$ is also an AF insulator at $x \approx 0.5$.

It is useful to compare our experimental findings with the results of the band structure calculations based on DFT (the Methods section; Supplementary Note 4; Supplementary Figs 8–10). Both the DFT and DFT + U calculations clearly predict the paramagnetic phase of $\text{NaFe}_{0.5}\text{Cu}_{0.5}\text{As}$ to be a metal (Supplementary Fig. 9). By contrast, our measurements have shown that the insulating behaviour of the resistivity persists above the Néel temperature (Fig. 1f), implying that $\text{NaFe}_{0.5}\text{Cu}_{0.5}\text{As}$ is a Mott insulator. This is also consistent with STM measurements on lower Cu-doping $\text{NaFe}_{1-x}\text{Cu}_x\text{As}$, where the overall line shape of the electronic spectrum at $x=0.3$ is similar to those of lightly electron-doped copper oxides close to the parent Mott insulator²¹.

To understand the origin of the Mott-insulating behaviour, we address how Cu doping affects the strength of electron correlations (the Methods section; Supplementary Note 5; Supplementary Figs 11 and 12). Our starting point is that the local (ionization) potential difference between the Fe and Cu ions, as illustrated in Fig. 4a and described by the energy shift Δ in Fig. 4b, will suppress the hopping integral between Fe and Cu sites. This causes a reduction in the kinetic energy or, equivalently, the electron bandwidth. The ratio of the on-site Coulomb repulsion U (including the Hund's coupling J_H) relative to the bandwidth will effectively increase, even if the raw values of U and J_H remain the same as in pure NaFeAs . This would enhance the tendency of electron localization even without considering the disorder effects with increasing x (refs 37,38).

The case of $x=0.5$ allows a detailed theoretical analysis. Here, the Cu and Fe ions in $\text{NaFe}_{1-x}\text{Cu}_x\text{As}$ have real space ordering, as discussed above. We study the metal-insulator transition in multi-orbital Hubbard models for $\text{NaFe}_{0.5}\text{Cu}_{0.5}\text{As}$ via the $U(1)$ slave-spin mean-field theory³⁰. We use the tight-binding parameters for NaFeAs , and consider the limit of a large local potential difference between Cu and Fe, which transfers charge from Fe to Cu to Cu^{1+} ($n=10$). The fully occupied Cu $3d$ shell makes the Cu ions essentially as vacancies. Reduction of the Fe $3d$ electron bandwidth is caused by this kinetic blocking effect (Supplementary Fig. 11). The resulting ground-state phase diagram is shown in Fig. 4c. For realistic parameters, illustrated by the shaded region, a Mott localization takes place. Our understanding is in line with the general theoretical identification of a Mott-insulating phase in an overall phase diagram³⁰, which takes into account a kinetic energy reduction induced increase of the effective interactions and a decrease of the $3d$ electron-filling from 6 per Fe^{2+} to 5 per Fe^{3+} (refs 7,9–11,30).

Our work uncovers a Mott insulator, $\text{NaFe}_{0.5}\text{Cu}_{0.5}\text{As}$, and provides its understanding in an overall phase diagram of both bandwidth and electron-filling controls³⁰. Our results suggest that

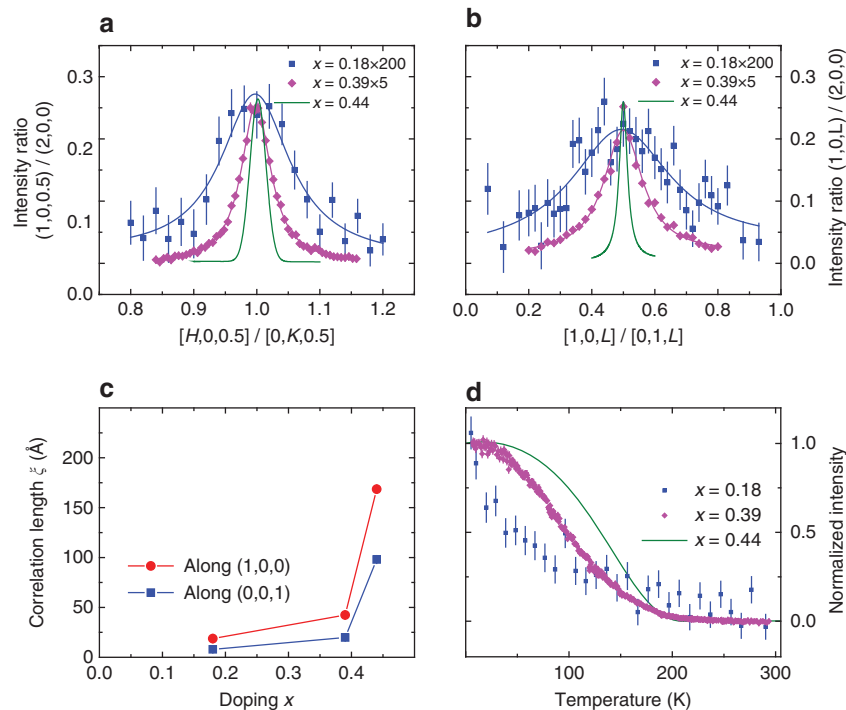


Figure 3 | Cu-doping evolution of the magnetic order in NaFe_{1-x}Cu_xAs. (a) Comparison of wave vector scans along the $[H, 0, 0.5]/[0, K, 0.5]$ direction for NaFe_{1-x}Cu_xAs single crystals with $x = 0.18, 0.39$ and 0.44 . The data are normalized to the $(2, 0, 0)$ nuclear Bragg peak. Note that intensity in the $x = 0.18$ and 0.39 samples are multiplied by 200 and 5 times, respectively. (b) Similar scans along the $[1, 0, L]/[0, 1, L]$ direction. (c) Cu-doping evolution of the spin-spin correlation length. The correlation length along $(1, 0, 0)$ for the $x = 0.44$ sample is resolution limited. (d) Cu-doping evolution of the magnetic order parameter for NaFe_{1-x}Cu_xAs. All error bars represent statistical error (1 s.d.).

the electron correlations of the iron pnictides, while weaker than those of the iron chalcogenides, are sufficiently strong to place these materials in proximity to the Mott localization. This finding makes it natural that the electron correlations and the associated bad-metal behaviour and magnetism induce a similarly high superconducting transition temperature in the iron pnictides as in the iron chalcogenide family. Such a commonality, in spite of the very different chemical composition and electronic structure of these two broad classes of materials, introduces considerable simplicity in the quest for a unified framework of the iron-based superconductivity. More generally, the proximity to the Mott transition links the superconductivity of the iron pnictides to that arising in the copper oxides, organic charge-transfer salts³⁹ and alkali-doped fullerides⁴⁰, and suggests that the same framework may apply to all these strongly correlated electronic systems.

Note added after submission: very recently, angle-resolved photoemission spectroscopy measurements on NaFe_{0.56}Cu_{0.44}As samples also confirmed its Mott-insulating nature⁴¹.

Methods

Sample preparation and experimental details. NaFe_{1-x}Cu_xAs single crystals were grown by the self-flux method using the same growth procedure as for NaFe_{1-x}Co_xAs described in earlier work⁴². The Cu-doping levels used in this paper were determined by inductively coupled plasma atomic-emission spectroscopy. Samples with nominal Cu concentrations of $x = 2, 20, 50, 75$ and 90% were prepared, resulting in actual Cu concentrations of $x = 1.6, 18.4(0.4), 38.9(2.8), 44.2(1.7)$ and $48.4(3.4)\%$. For each nominal doping except $x = 2\%$, five to six samples were measured and the s.d. in these measurements are taken as the uncertainty of the actual concentrations. For simplicity, the actual concentrations are noted as $x = 1.6, 18, 39, 44$ and 48% in the rest of the paper. This suggests that the solubility limit of Cu in NaFe_{1-x}Cu_xAs single crystals by our growth method is $\approx 50\%$.

For resistivity measurements, samples were mounted onto a resistivity puck inside an Ar filled glove box by the four-probe method and covered in Apiezon N grease. The prepared puck is then transferred in an Ar-sealed bottle and is only briefly exposed in air, while being loaded into a physical property measurement

system for measurements. After measurements, no visual deterioration of the samples were seen under a microscope.

For single-crystal elastic neutron scattering measurements, samples were covered with a hydrogen-free glue and then stored in a vacuum bottle at all times except during sample loading before the neutron scattering experiment. While our largest crystals grown are up to 2 g, we typically used thin plate-like samples $\sim 5 \times 5 \text{ mm}^2$ in size with mass $\approx 0.2 \text{ g}$ for elastic neutron scattering measurements. Measurement of the sample with $x = 0.18$ was carried out on the N5 triple-axis spectrometer at the Canadian Neutron Beam Center, Chalk River Laboratories. Pyrolytic graphite (PG) monochromator and analyser ($E_i = 14.56 \text{ meV}$) were used with none-36'-sample-33'-144' collimation set-up. A PG filter was placed after the sample to eliminate contamination from higher-order neutron wavelengths. The experiment on $x = 0.39$ and 0.44 samples were done on the HB-3 triple-axis spectrometer and the HB-1A fixed-incident-energy triple-axis spectrometer, respectively, at the High Flux Isotope Reactor, Oak Ridge National Laboratory. On HB-3, a PG monochromator ($E_i = 14.7 \text{ meV}$), analyser and two PG filters (one before and the other after the sample) were used with collimation set-up 48'-60'-sample-80'-120'. HB-1A uses two PG monochromators ($E_i = 14.6 \text{ meV}$) and two PG filters (mounted before and after second monochromator), resulting in negligible higher-order wavelengths neutrons in the incident beam. A PG analyser is placed after the sample. The collimation used was 48'-48'-sample-40'-68'. In all cases above, the samples were aligned in $[H, 0, L]$ scattering plane.

The polarized single-crystal neutron scattering measurements were carried out on the C5 polarized beam triple-axis spectrometer at Canadian Neutron Beam Center, Chalk River Laboratories. The neutron beams were polarized with Heusler (1, 1, 1) crystals with a vertically focusing monochromator and a flat analyser ($E_i = 13.70 \text{ meV}$). A PG filter was placed after the sample and none-48'-51'-144' collimation was used. Neutron polarization was maintained by using permanent magnet guide fields. Mezei flippers were placed before the sample to allow the measurement of neutron SF and NSF scattering cross-sections. A 5-coil Helmholtz assembly was used to control the neutron spin orientation at the sample position by producing a magnetic field of the order of 10 G. The orientation of the magnetic field at the sample position was automatically adjusted to allow the measurements to be performed for the neutron spin to be parallel or perpendicular to the momentum transfer. The flipping ratio, defined as the ratio of nuclear Bragg peak intensities in NSF and SF channels, was measured to be $\sim 10:1$ for various field configurations. The sample was studied in both $[H, 0, L]$ and $[H, H, L]$ scattering planes.

The XAS and RIXS measurements on the $x = 0.44$ samples were carried out at the Advanced Resonant Spectroscopy beamline of the Swiss Light Source, Paul Scherrer Institut, Switzerland⁴³. Samples were cleaved *in situ* and measured in a

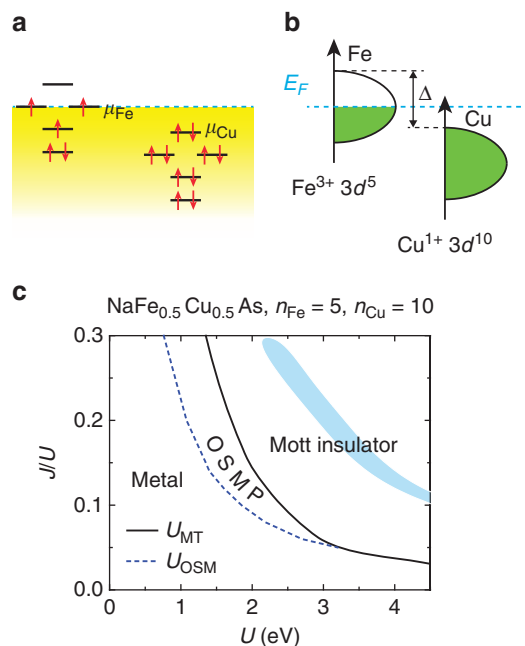


Figure 4 | Schematic 3d electronic states and parameter regimes of a Mott insulator in the theoretical phase diagram for NaFe_{0.5}Cu_{0.5}As.

Schematic of the electronic states of a Cu ion alongside those of an Fe ion, shown in terms of the atomic levels (a) and the electronic density of states (b). The relative potential difference associated with the two ions is specified in terms of an energy shift, Δ , as illustrated in b. (c) The ground-state phase diagram of a multi-orbital Hubbard model for NaFe_{0.5}Cu_{0.5}As. U_{OSM} and U_{MT} refer to the critical U values for an orbital-selective Mott (OSM) transition and a Mott transition (MT), respectively into an orbital-selective Mott phase (OSMP) and a Mott insulator. The shaded region shows the physical parameter regime as determined by comparing the theoretically calculated bandwidth renormalization factors of the three t_{2g} orbitals with those determined by the angle-resolved photoemission spectroscopy (ARPES) results (Supplementary Note 5).

vacuum better than 1×10^{-10} mbar. X-ray absorption was measured in total electron yield mode by recording the drain current from the samples and in total fluorescence yield with a photodiode. Linearly polarized X-rays with $E = 931.8$ eV resonant at the Cu L_3 edge were used for the RIXS measurements. The total momentum transfer was kept constant, but the component of momentum transfer in the ab plane has been varied.

For neutron powder diffraction measurements, the samples were ground from 2 g ($x = 0.016, 0.18, 0.39$ and 0.44) of single crystals and sealed in vanadium sample cans inside a He-filled glove box. Neutron powder diffraction measurements were carried out at room temperature (300 K) on the BT1 high-resolution powder diffractometer at NIST Center for Neutron Research. The Ge(3, 1, 1) monochromator was used to yield the highest neutron intensity and best resolution at low scattering angles. For the $x = 0.44$ sample, measurement at 4 K using a Cu(3, 1, 1) monochromator was also carried out.

For the single-crystal neutron diffraction measurement, a sample with $x = 0.44$ (25 mg) was used. The experiment was carried out at the four-circle diffractometer HB-3A at the High Flux Isotope Reactor, Oak Ridge National Laboratory. The data was measured at 250 K with neutron wavelength of 1.003 Å from a bent Si(3, 3, 1) monochromator using an Anger camera detector. Bragg peaks associated with the NaFeAs structure were measured with 1 s per point by carrying out rocking scans. Super-lattice peaks were measured with 10 min per point at each position.

DFT-based electronic structure calculations. To gain insight into the insulating nature of Cu-doped NaFeAs, we have performed a series of DFT-based electronic structure calculations. The electronic band structure calculations have been performed using a full-potential linear augmented plane-wave method as implemented in the WIEN2K package⁴⁴. The exchange-correlations function was taken within the generalized gradient approximation (GGA) in the parameterization of Perdew, Burke and Ernzerhof⁴⁵. For the atomic spheres, the muffin-tin radii (R_{MT}) were chosen to be 2.5 Bohr for Na sites, 2.38 Bohr for Fe and Cu, and 2.26 Bohr for As sites, respectively. The number of plane waves was limited by a cutoff parameter ($R_{MT} \times K_{max}$) = 7.5. To account for the on-site correlations in the form of the Hubbard parameter U , the GGA + U approach in a Hartree-Fock-like scheme was

used^{46,47}, with the value $U = 3.15$ eV as calculated in LiFeAs using the constrained random-phase approximation (RPA) approach⁴⁸.

While the neutron diffraction studies were performed on the $x = 0.44$ sample, it is much easier theoretically to study the 50% Cu-doped NaFe_{0.5}Cu_{0.5}As. To model the crystal structure, the experimentally determined lattice parameters and atomic coordinates of NaFe_{0.56}Cu_{0.44}As at 4 K were used (Supplementary Table 3). The difference between the structure at $x = 0.44$ and 0.5 was deemed inessential in view of the weak dependence of the lattice parameters on Cu concentration x (Supplementary Table 3). While the experimental structure can be fitted with a symmetry group $P4/nmm$ with disordered Cu/Fe, the high-resolution TEM measurements found that the super-lattice peaks indicate a stripe-like ordered pattern (Fig. 1d) consistent with the space group $Ibam$. We have therefore used the $Ibam$ space group, with four formula units per unit cell, to perform the *ab initio* calculations. Interestingly, the results of the calculations turn out to be insensitive to the details of the atomic arrangement: for instance, arranging Cu/Fe atoms in the checkerboard pattern results in a very similar density of states as that obtained for the stripe-like atomic configuration. We also note that the adopted ordered arrangement of Fe/Cu sites neglects the effects of disorder and Anderson localization, which may be important at low doping levels $x < 0.5$. Those effects are however beyond the grasp of the first principles DFT calculations.

U(1) slave-spin mean-field theory. To take into account the correlation effects beyond the Hartree-Fock level, we further study the metal-insulator transition in multi-orbital Hubbard models for both NaFeAs and NaFe_{0.5}Cu_{0.5}As via the U(1) slave-spin mean-field theory⁴⁹. The model Hamiltonian contains a tight-binding part and a local interaction part. Detailed description of the model is given in ref. 49. The tight-binding parameters for NaFeAs are taken from ref. 50, and the electron density is fixed to $n = 6$ per Fe. As for NaFe_{0.5}Cu_{0.5}As, the very large local potential difference between Cu and Fe, as estimated from our and previous³⁷ DFT calculations, leads to charge transferring from Fe to Cu. As a result, Fe is effectively hole doped when the Cu-doping concentration is close to 0.5. This picture is supported by our experimental results which suggest that the Cu is in a $3d^{10}$ configuration with $n = 10$, and Fe configuration is $3d^5$ with $n = 5$. As a zeroth-order approximation to the fully occupied Cu $3d$ shell, we treat Cu ions as vacancies. They organize themselves in a columnar-order pattern in NaFe_{0.5}Cu_{0.5}As, as shown in Fig. 1d.

Data availability. The data that support the findings of this study are available from the corresponding authors on request.

References

- Kamihara, Y., Watanabe, T., Hirano, M. & Hosono, H. Iron-based layered superconductor La[O_{1-x}F_x]FeAs ($x = 0.05 - 0.12$) with $T_c = 26$ K. *J. Am. Chem. Soc.* **130**, 3296–3297 (2008).
- Stewart, G. R. Superconductivity in iron compounds. *Rev. Mod. Phys.* **83**, 1589–1652 (2011).
- Scalapino, D. J. A common thread: the pairing interaction for the unconventional superconductors. *Rev. Mod. Phys.* **84**, 1383 (2012).
- Dai, P. C. Antiferromagnetic order and spin dynamics in iron based superconductors. *Rev. Mod. Phys.* **87**, 855 (2015).
- Si, Q., Yu, R. & Abrahams, E. High temperature superconductivity in iron pnictides and chalcogenides. *Nat. Rev. Mater.* **1**, 16017 (2016).
- Yin, Z. P., Haule, K. & Kotliar, G. Kinetic frustration and the nature of the magnetic and paramagnetic states in iron pnictides and iron chalcogenides. *Nat. Mater.* **10**, 932–935 (2011).
- Si, Q. & Abrahams, E. Strong correlations and magnetic frustration in the high T_c iron pnictides. *Phys. Rev. Lett.* **101**, 076401 (2008).
- Qazilbash, M. M. *et al.* Electronic correlations in the iron pnictides. *Nat. Phys.* **5**, 647–650 (2009).
- Ishida, H. & Liebsch, A. Fermi-liquid, non-Fermi-liquid, and Mott phases in iron pnictides and cuprates. *Phys. Rev. B* **81**, 054513 (2010).
- Misawa, T., Nakamura, K. & Imada, M. *Ab initio* evidence for strong correlations associated with mott proximity in iron-based superconductors. *Phys. Rev. Lett.* **108**, 177007 (2012).
- de' Medici, L., Giovannetti, G. & Capone, M. Selective Mott physics as a key to iron superconductors. *Phys. Rev. Lett.* **112**, 177001 (2014).
- Mazin, I. I. Superconductivity gets an iron boost. *Nature* **464**, 183–186 (2010).
- Hirschfeld, P. J., Korshunov, M. M. & Mazin, I. I. Gap symmetry and structure of Fe-based superconductors. *Rep. Prog. Phys.* **74**, 124508 (2011).
- Chubukov, A. V. Pairing mechanism in Fe-based superconductors. *Annu. Rev. Condens. Matter Phys.* **3**, 57–92 (2012).
- Zhu, J.-X. *et al.* Band narrowing and Mott localization in iron oxychalcogenides La₂O₂Fe₂O(Se,S). *Phys. Rev. Lett.* **104**, 216405 (2010).
- Fang, M. H. *et al.* Fe-based superconductivity with $T_c = 31$ K bordering an antiferromagnetic insulator in (Ti,K)Fe₂Se₂. *Europhys. Lett.* **94**, 27009 (2011).
- Katasea, T., Hiramatsu, H., Kamiya, T. & Hosono, H. Electric double-layer transistor using layered iron selenide Mott insulator TlFe_{1.6}Se₂. *Proc. Natl Acad. Sci. USA* **111**, 3979–3983 (2014).

18. Chen, T.-K. *et al.* Fe-vacancy order and superconductivity in tetragonal β -Fe_{1-x}Se. *Proc. Natl Acad. Sci. USA* **111**, 63–68 (2014).
19. Yi, M. *et al.* Observation of temperature-induced crossover to an orbital-selective Mott phase in A_xFe_{2-y}Se₂ (A = K, Rb) superconductors. *Phys. Rev. Lett.* **110**, 067003 (2013).
20. Wang, A. F. *et al.* Phase diagram and physical properties of NaFe_{1-x}Cu_xAs single crystals. *Phys. Rev. B* **88**, 094516 (2013).
21. Ye, C. *et al.* Strong similarities between the local electronic structure of insulating iron pnictide and lightly doped cuprate. *Phys. Rev. X* **5**, 021013 (2015).
22. Li, S. *et al.* Structural and magnetic phase transitions in Na_{1-δ}FeAs. *Phys. Rev. B* **80**, 020504 (R) (2009).
23. Tan, G. T. *et al.* Electron doping evolution of structural and antiferromagnetic phase transitions in NaFe_{1-x}Co_xAs iron pnictides. *Phys. Rev. B* **94**, 014509 (2016).
24. Pfisterer, M. & Nagorsen, G. On the structure of ternary arsenides. *Z. Naturforsch. B* **35B**, 703–704 (1980).
25. Anand, V. K. *et al.* Crystal growth and physical properties of SrCu₂As₂, SrCu₂Sb₂, and BaCu₂Sb₂. *Phys. Rev. B* **85**, 214523 (2012).
26. Yan, Y. J. *et al.* Structural, magnetic, and electronic transport properties of hole-doped SrFe_{2-x}Cu_xAs₂ single crystals. *Phys. Rev. B* **87**, 075105 (2013).
27. McLeod, J. A. *et al.* Electronic structure of copper pnictides: influence of different cations and pnictogens. *Phys. Rev. B* **88**, 014508 (2013).
28. Takeda, H. *et al.* Cu substitution effects on the local magnetic properties of Ba(Fe_{1-x}Cu_x)₂As₂: a site-selective ⁷⁵As and ⁶³Cu NMR study. *Phys. Rev. Lett.* **113**, 117001 (2014).
29. Singh, D. J. Electronic structure of BaCu₂As₂ and SrCu₂As₂: *sp*-band metals. *Phys. Rev. B* **79**, 153102 (2009).
30. Yu, R., Zhu, J.-X. & Si, Q. Orbital-dependent effects of electron correlations in microscopic models for iron-based superconductors. *Curr. Opin. Solid State Mater. Sci.* **17**, 65–71 (2013).
31. Song, Y. *et al.* In-plane spin excitation anisotropy in the paramagnetic state of NaFeAs. *Phys. Rev. B* **88**, 134512 (2013).
32. Moon, R. M., Riste, T. & Koehler, W. C. Polarization analysis of thermal-neutron scattering. *Phys. Rev.* **181**, 920–931 (1969).
33. Hiraishi, M. *et al.* Bipartite magnetic parent phases in the iron oxypnictide superconductor. *Nat. Phys.* **10**, 300–303 (2014).
34. Williams, A. J., McQueen, T. M., Ksenofontov, V., Felser, C. & Cava, R. J. The metal-insulator transition in Fe_{1.01-x}Cu_xSe. *J. Phys. Condens. Matter* **21**, 305701 (2009).
35. Huang, T.-W. *et al.* Doping-driven structural phase transition and loss of superconductivity in M_xFe_{1-x}Se₂ (M = Mn, Cu). *Phys. Rev. B* **82**, 104502 (2010).
36. Chadov, S. *et al.* Electronic structure, localization, and spin-state transition in Cu-substituted FeSe: Fe_{1-x}Cu_xSe. *Phys. Rev. B* **81**, 104523 (2010).
37. Wadati, H., Elfmov, I. & Sawatzky, G. A. Where are the extra *d* electrons in transition-metal substituted Fe pnictides? *Phys. Rev. Lett.* **105**, 157004 (2010).
38. Berlijn, T., Lin, C.-H., Garber, W. & Ku, W. Do Transition metal substitutions dope carriers in iron based superconductors? *Phys. Rev. Lett.* **108**, 207003 (2012).
39. Lee, P. A., Nagaosa, N. & Wen, X. G. Doping a Mott insulator: physics of high-temperature superconductivity. *Rev. Mod. Phys.* **78**, 17–85 (2006).
40. Takabayashi, Y. *et al.* The disorder-free non-BCS superconductor Cs₃C₆₀ emerges from an antiferromagnetic insulator parent state. *Science* **323**, 1585–1590 (2009).
41. Matt, C. E. *et al.* NaFe_{0.56}Cu_{0.44}As: a pnictide insulating phase induced by on-site coulomb interaction. *Phys. Rev. Lett.* **117**, 097001 (2016).
42. Tanatar, M. A. *et al.* Evolution of normal and superconducting properties of single crystals of Na_{1-δ}FeAs upon interaction with environment. *Phys. Rev. B* **85**, 014510 (2012).
43. Strocov, V. N. *et al.* High-resolution soft X-ray beamline ADDRESS at the Swiss Light Source for resonant inelastic X-ray scattering and angle-resolved photoelectron spectroscopies. *J. Synchrotron Radiat.* **17**, 631–643 (2010).
44. Blaha, P., Schwarz, K., Madsen, G. K. H., Kvasnicka, D. & Luitz, J. in *An Augmented Plane Wave and Local Orbitals Program for Calculating Crystal Properties* (ed. Schwarz K.) (Technical University of Wien, 2001).
45. Perdew, J. P., Burke, K. & Ernzerhof, M. Generalized gradient approximation made simple. *Phys. Rev. Lett.* **77**, 3865–3868 (1996).
46. Anisimov, V. I., Zaanen, J. & Andersen, O. K. Band theory and Mott insulators: Hubbard *U* instead of Stoner *I*. *Phys. Rev. B* **44**, 943–954 (1991).
47. Liechtenstein, A. I., Anisimov, V. I. & Zaanen, J. Density-functional theory and strong interactions: orbital ordering in Mott-Hubbard insulators. *Phys. Rev. B* **52**, R5467 (1995).
48. Miyake, T., Nakamura, K., Arita, R. & Imada, M. Comparison of *ab initio* low-energy models for LaFePO, LaFeAsO, BaFe₂As₂, LiFeAs, FeSe, and FeTe: electron correlation and covalency. *J. Phys. Soc. Jpn* **79**, 044705 (2010).
49. Yu, R. & Si, Q. *U*(1) slave-spin theory and its application to Mott transition in a multiorbital model for iron pnictides. *Phys. Rev. B* **86**, 085104 (2012).
50. Yu, R., Zhu, J.-X. & Si, Q. Orbital-selective superconductivity, gap anisotropy, and spin resonance excitations in a multiorbital *t*-*J*₁-*J*₂ model for iron pnictides. *Phys. Rev. B* **89**, 024509 (2014).

Acknowledgements

We thank X.H. Chen, B.J. Campbell and Lijun Wu for helpful discussions, Leland Harriger, Scott Carr, Weiyi Wang and Binod K. Rai for assisting with some experiments. The single-crystal growth and neutron scattering work at Rice is supported by the U.S. DOE, BES under contract no. DE-SC0012311 (P.D.). A part of the material synthesis work at Rice is supported by the Robert A. Welch Foundation Grant No. C-1839 (P.D.). The theoretical work at Rice was in part supported by the Robert A. Welch Foundation Grant No. C-1818 (A.H.N.), C-1411 (Q.S.), by U.S. NSF grants DMR-1350237 (A.H.N.) and DMR-1611392 (Q.S.), and by the Alexander von Humboldt Foundation (Q.S.). E.M. and J.C. acknowledge support from the DOD PECASE. The electron microscopy study at Brookhaven National Laboratory was supported by the U.S. DOE, BES, by the Materials Sciences and Engineering Division under Contract No. DE-AC02-98CH10886. The use of ORNL's High Flux Isotope Reactor was sponsored by the Scientific User Facilities Division, Office of BES, U.S. DOE. XAS and RIXS experiments have been performed at the Advanced Resonant Spectroscopy beamline of the Swiss Light Source at the Paul Scherrer Institute. T.S. and M.D. acknowledge funding through the Swiss National Science Foundation within the D-A-CH programme (SNSF Research Grant 200021L 141325). R.Y. acknowledges the support from the National Science Foundation of China Grant number 11374361, and the Fundamental Research Funds for the Central Universities and the Research Funds of Remnin University of China Grant number 14XNLF08. C.C. acknowledges the support from the National Natural Science Foundation of China Grant No. 51471135, the National Key Research and Development Program of China Grant No. 2016YFB1100101 and Shaanxi International Cooperation Program.

Author contributions

Most of the single-crystal growth and neutron scattering experiments were carried out by Y.S. with assistance from C.C., Y.L., C.Z., Q.H., H.W., W.T., S.C. and H.C. The polarized neutron scattering experiments were performed by Z.Y. TEM measurements were carried out by J.T. and Y.Z. Transport and inductively coupled plasma measurements were carried out by C.C. and J.S.C., under the supervision of E.M. The XAS and RIXS experiments were performed by Y.-B.H., M.D. and T.S. The theoretical work was done by R.Y., A.H.N. and Q.S. P.D. provided the overall lead of the project. The paper was written by P.D., Y.S., A.H.N., R.Y. and Q.S. All authors provided comments.

Additional information

Supplementary Information accompanies this paper at <http://www.nature.com/naturecommunications>

Competing financial interests: The authors declare no competing financial interests.

Reprints and permission information is available online at <http://npg.nature.com/reprintsandpermissions/>

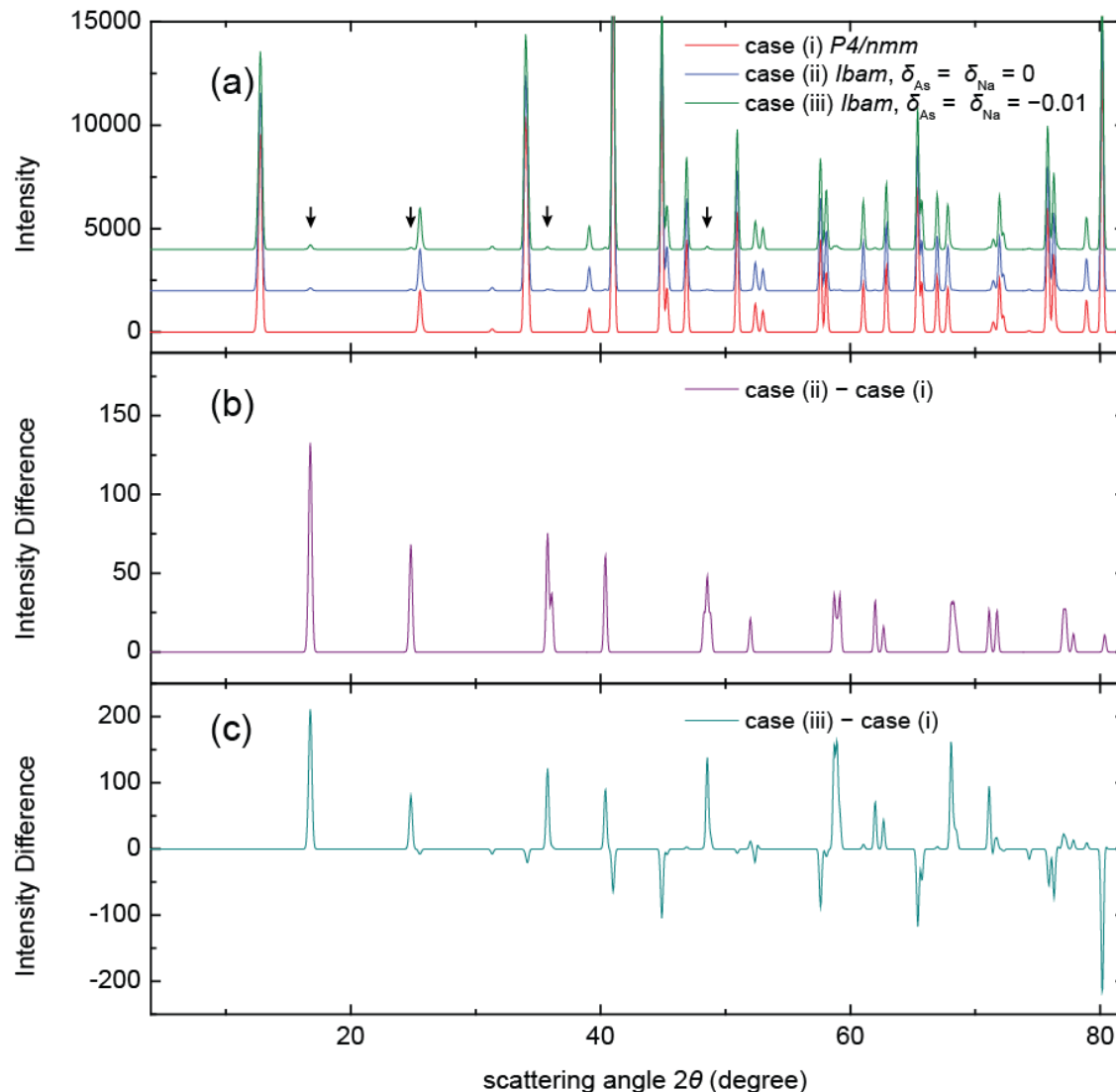
How to cite this article: Song, Y. *et al.* A Mott insulator continuously connected to iron pnictide superconductors. *Nat. Commun.* **7**, 13879 doi: 10.1038/ncomms13879 (2016).

Publisher's note: Springer Nature remains neutral with regard to jurisdictional claims in published maps and institutional affiliations.

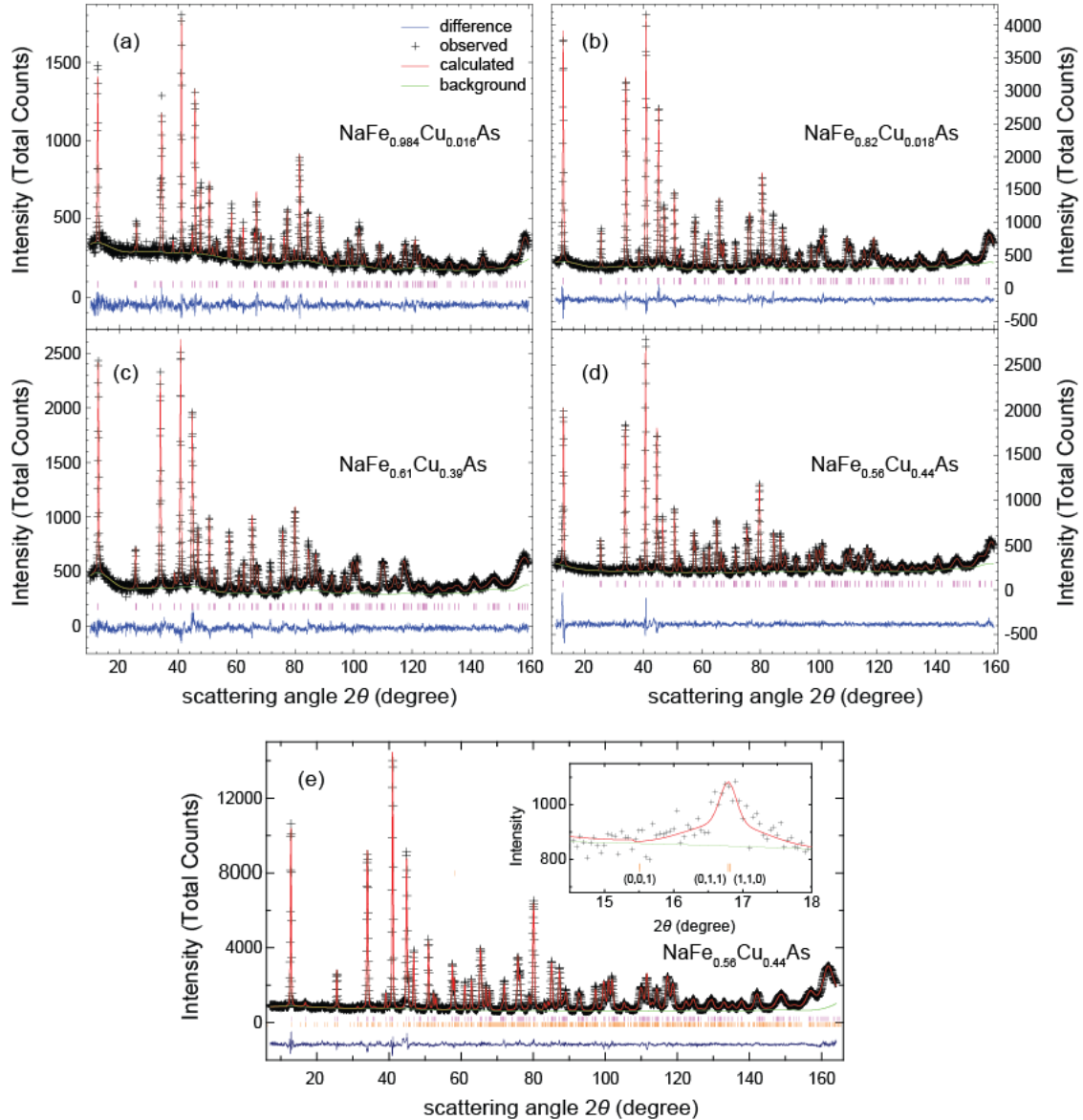


This work is licensed under a Creative Commons Attribution 4.0 International License. The images or other third party material in this article are included in the article's Creative Commons license, unless indicated otherwise in the credit line; if the material is not included under the Creative Commons license, users will need to obtain permission from the license holder to reproduce the material. To view a copy of this license, visit <http://creativecommons.org/licenses/by/4.0/>

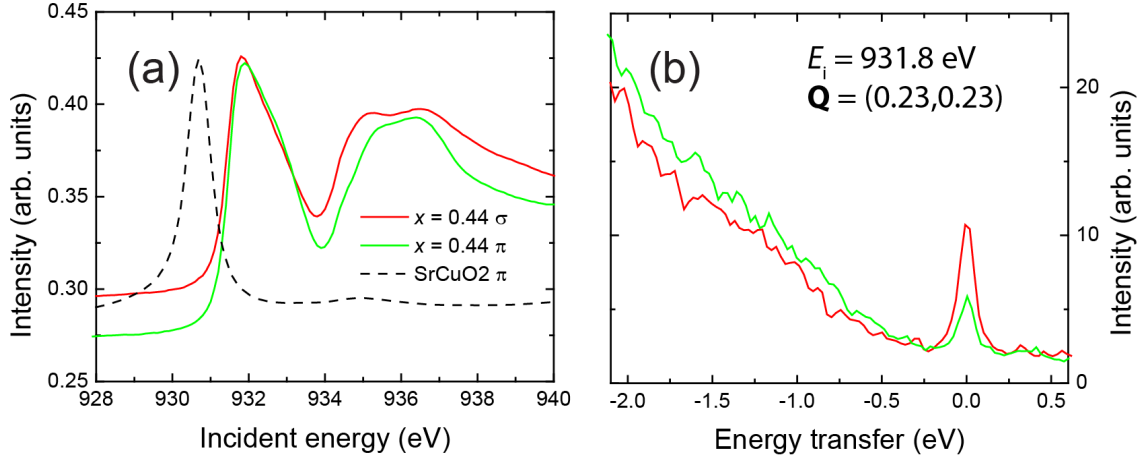
© The Author(s) 2016



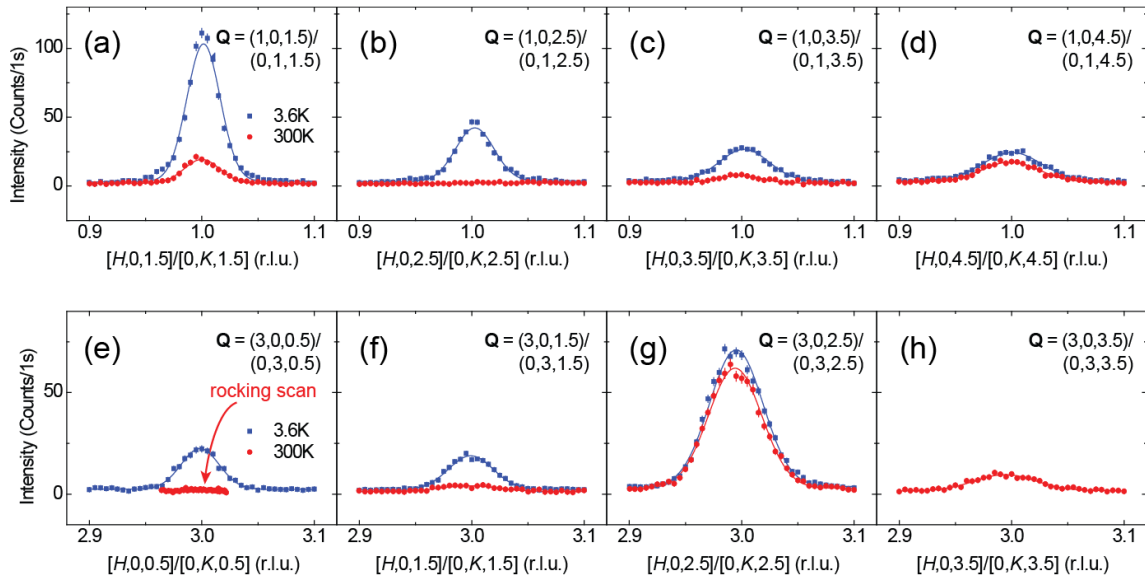
Supplementary Figure 1: Calculated neutron powder diffraction profiles for $\text{NaFe}_{0.5}\text{Cu}_{0.5}\text{As}$. (a) Case (i) where Fe and Cu are completely disordered and $\delta_{As} = \delta_{Na} = 0$, corresponding to the $P4/nmm$ space group when $a = c$ ($Ibam$ notation). Case (ii) has Fe-Cu stripe order and $\delta_{As} = \delta_{Na} = 0$, case (iii) further has non-zero δ_{As} and δ_{Na} . The black arrows mark some super-lattice peak positions. (b) Difference between case (ii) and case (i), when Fe and Cu order into stripes, only super-lattice peaks are formed without affecting nuclear Bragg peaks already present in case (i). (c) Difference between case (iii) and case (i), having non-zero δ_{As} and δ_{Na} only slightly affects the intensities of nuclear peaks already present in case (i). Note the intensity range is much smaller in (b) and (c) compared to (a).



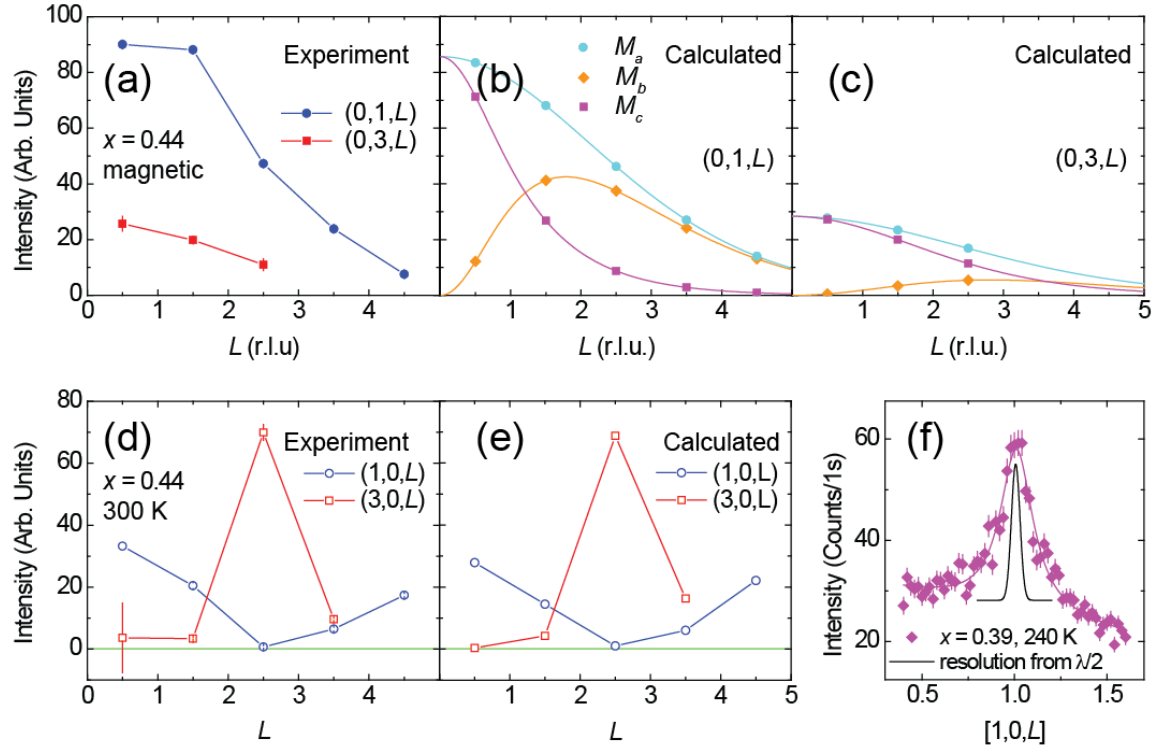
Supplementary Figure 2: Neutron powder diffraction data for $\text{NaFe}_{1-x}\text{Cu}_x\text{As}$ measured at 300K and 4K. (a) Observed (black crosses) and calculated (red lines) neutron powder diffraction intensities for $\text{NaFe}_{0.984}\text{Cu}_{0.016}\text{As}$ at 300 K using space group $P4/nmm$. Short magenta vertical lines represent nuclear Bragg peak positions, the blue trace is the difference between measured and calculated intensities. (b), (c) and (d) show similar results for $\text{NaFe}_{1-x}\text{Cu}_x\text{As}$ with $x = 0.18, 0.39$ and 0.44 respectively. Despite the observation of super-lattice peaks in samples with $x = 0.39$ and 0.44 at 300K, such peaks are not visible in neutron powder diffraction data and all data sets at 300K are fit with the same tetragonal structure as undoped NaFeAs in the paramagnetic state with space group $P4/nmm$. (e) $\text{NaFe}_{0.56}\text{Cu}_{0.44}\text{As}$ at 4K fit with $Ibam$ structure described in Supplementary Table 1 and the magnetic structure in Fig. 1(d), magenta vertical lines correspond to nuclear Bragg peak positions and orange vertical lines are magnetic Bragg peak positions. The inset zooms in on a super-lattice/magnetic peak.



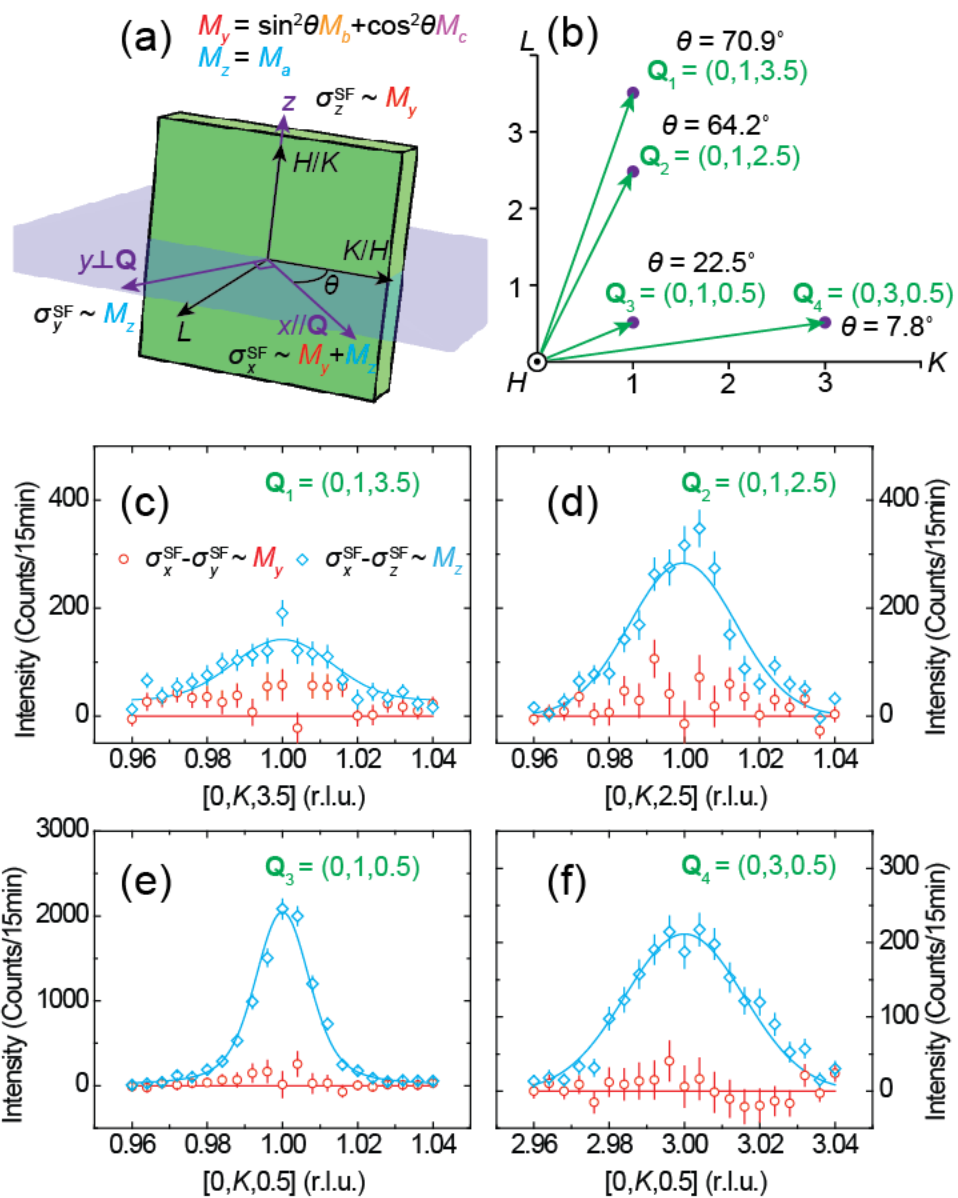
Supplementary Figure 3: XAS and RIXS measurements on $\text{NaFe}_{0.56}\text{Cu}_{0.44}\text{As}$. (a) X-ray absorption spectroscopy (XAS) measurements on $\text{NaFe}_{0.56}\text{Cu}_{0.44}\text{As}$ (solid lines) and SrCuO_2 (dashed line) obtained at 10 K. (b) Typical resonant inelastic X-ray scattering (RIXS) measurement on the same compound with incident energy $E_i = 931.8$ eV and in-plane momentum transfer $q_{\parallel} = 0.498 \text{ \AA}^{-1}$ obtained at 10 K. Light green lines are measurements with π polarization and red lines are corresponding measurements with σ polarization.



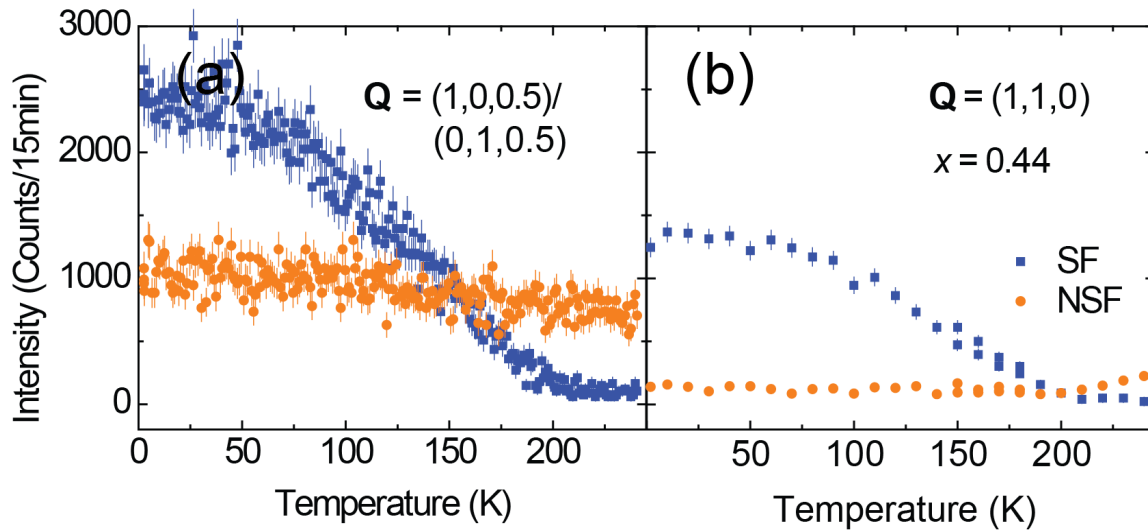
Supplementary Figure 4: Scans along $[H, 0, L]/[0, K, L]$ at wave-vectors equivalent to $(1, 0, 0.5)/(0, 1, 0.5)$ for $\text{NaFe}_{0.56}\text{Cu}_{0.44}\text{As}$ at 3.6 K and 300 K. These scans were measured with unpolarized neutrons. Scans at 3.6 K are shown as blue squares and scans measured at 300 K are shown as red circles. Scans centered at $\mathbf{Q} = (1, 0, L)/(0, 1, L)$ with $L = 1.5, 2.5, 3.5$ and 4.5 are respectively plotted in (a), (b), (c) and (d). Similarly scans centered at $\mathbf{Q} = (3, 0, L)/(0, 3, L)$ with $L = 0.5, 1.5, 2.5$ and 3.5 are shown in (e), (f), (g) and (h), respectively. Scan along $[H, 0, 0.5]/[0, K, 0.5]$ at 300 K for $\mathbf{Q} = (3, 0, 0.5)/(0, 3, 0.5)$ was not measured, instead a rocking scan is plotted to show that there is no observable intensity at this wave-vector and temperature. Scan along $[H, 0, 3.5]/[0, K, 3.5]$ at 3.6 K centered at $\mathbf{Q} = (3, 0, 3.5)/(0, 3, 3.5)$ was not measured. All vertical error bars represent statistical error (1 s. d.).



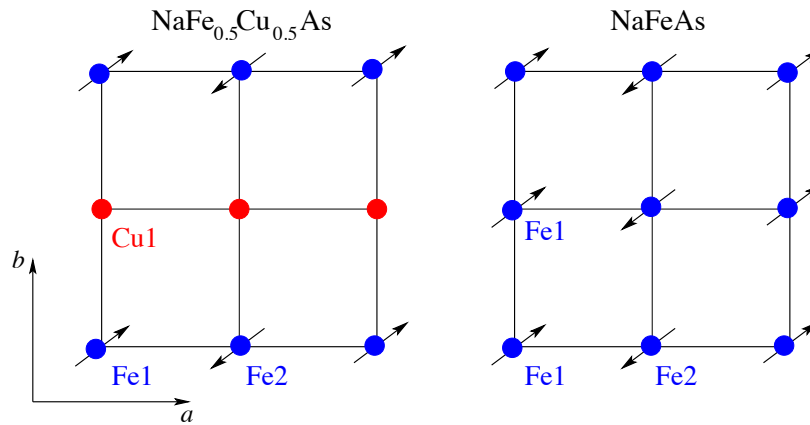
Supplementary Figure 5: Wave vector dependence of super-lattice peaks and magnetic peaks. (a) The magnetic intensities for equivalent wave-vectors $(0, 1, L)$ (solid blue circles) and $(0, 3, L)$ (solid red squares) are summarized for $\text{NaFe}_{0.56}\text{Cu}_{0.44}\text{As}$. The intensities were obtained from rocking scans at 3.6 K, correcting for contributions from super-lattice peaks estimated from $[H, 0, L]/[0, K, L]$ scans presented in Supplementary Figure 4. (b) Assuming Fe^{2+} magnetic form factor, the expected intensities for $(0, 1, L)$ wave-vectors are shown depending on the orientation of the magnetic moment. The magnetic moment along a axis (orange diamonds), b axis (cyan circles) and c axis (magenta squares) are compared. (c) Expected magnetic intensities are similarly shown for $(0, 3, L)$. (d) Super-lattice peak intensities for equivalent wave-vectors $(1, 0, L)$ (empty red squares) and $(3, 0, L)$ (empty blue circles) obtained from scans at 300 K in Figure S4, (e) shows the corresponding calculated intensity for $\text{NaFe}_{0.56}\text{Cu}_{0.44}\text{As}$ using the structure in Supplementary Table 1. (f) Scan along the $[1, 0, L]$ direction for $\text{NaFe}_{0.61}\text{Cu}_{0.39}\text{As}$ at 240 K (magenta diamonds), the instrument resolution (black line) is obtained by performing the same scan after removing the filters. Vertical error bars in (a), (d) and (e) are from least-square fits (1 s. d.). Vertical error bars in (f) represent statistical error (1 s. d.).



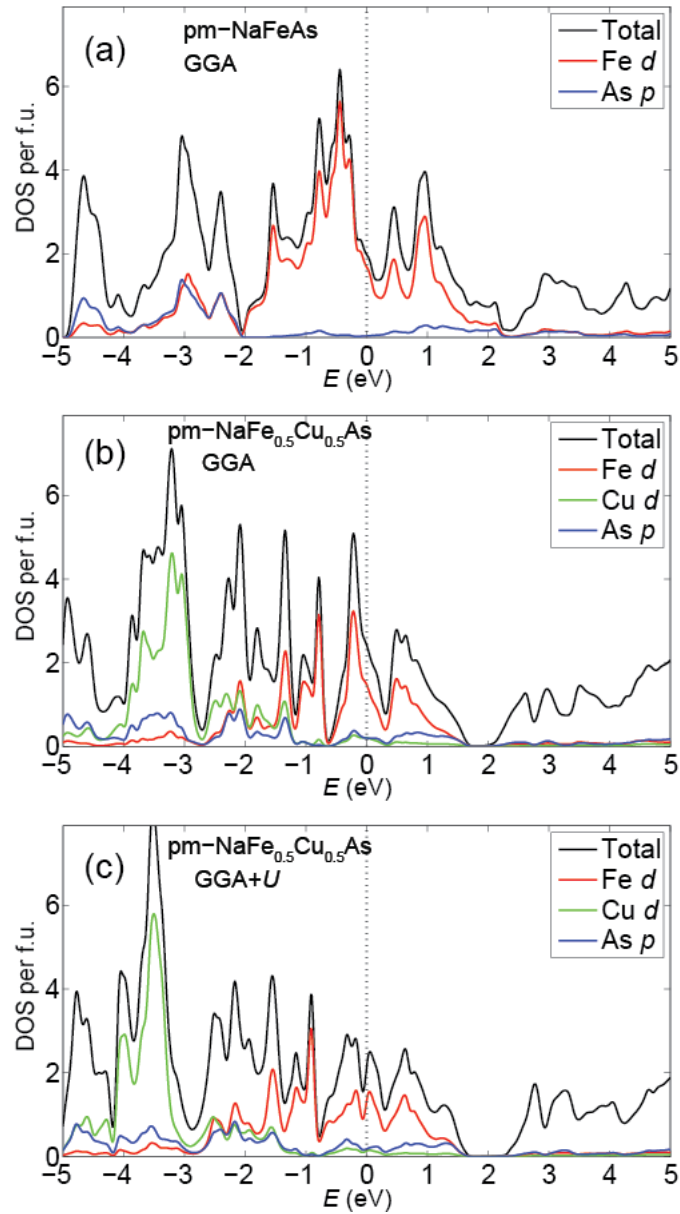
Supplementary Figure 6: Determining the spin direction using polarized neutron scattering. (a) Definition of x , y and z directions with respect to the crystallographic axes. (b) Wave vectors probed in $[0,K,L]$ scattering plane and the corresponding θ . M_y (open red circles) and M_z (open cyan diamonds) for $\mathbf{Q}_1 = (0,1,3.5)$, $\mathbf{Q}_2 = (0,1,2.5)$, $\mathbf{Q}_3 = (0,1,0.5)$ and $\mathbf{Q}_4 = (0,3,0.5)$ are shown in (c), (d), (e) and (f), respectively. All vertical error bars represent statistical error (1 s. d.).



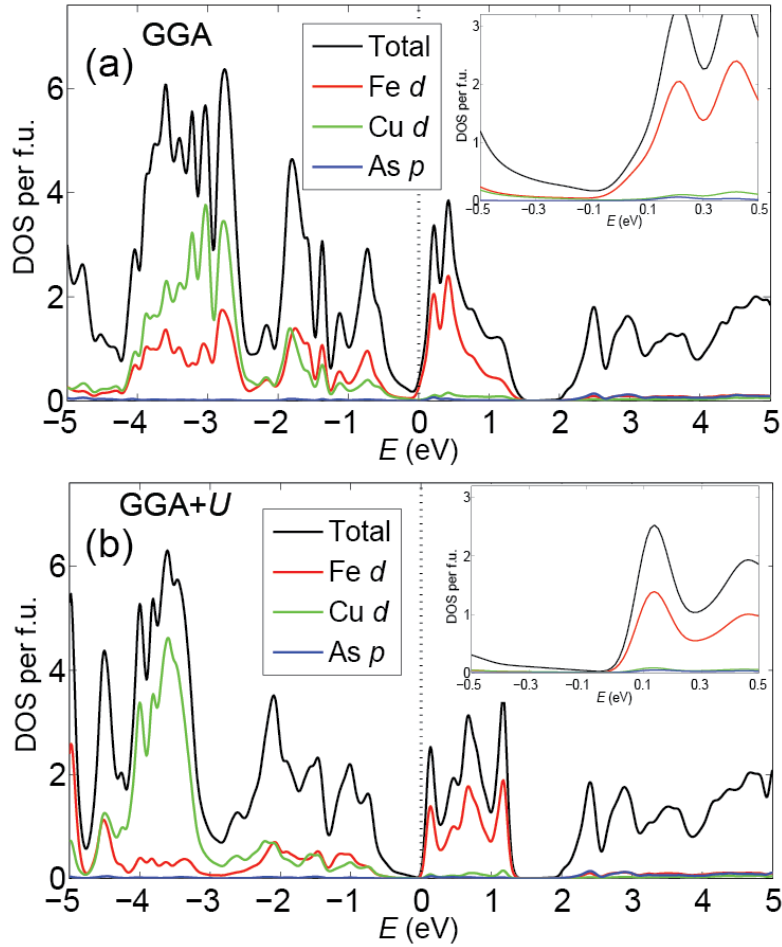
Supplementary Figure 7: Temperature dependence of magnetic and super-lattice peaks in $\text{NaFe}_{1-x}\text{Cu}_x\text{As}$. (a) Temperature dependence of SF (blue squares) and NSF (orange circles) channels for $\text{NaFe}_{0.56}\text{Cu}_{0.44}\text{As}$ at $Q = (1,0,0.5)/(0,1,0.5)$. Magnetic signal coming from $Q = (0,1,0.5)$ is seen in the SF channel whereas super-lattice signal coming from $Q = (1,0,0.5)$ are seen in the NSF signal. (b) Similar temperature dependence of SF and NSF channels at $Q = (1,1,0)$. All vertical error bars represent statistical error (1 s. d.).



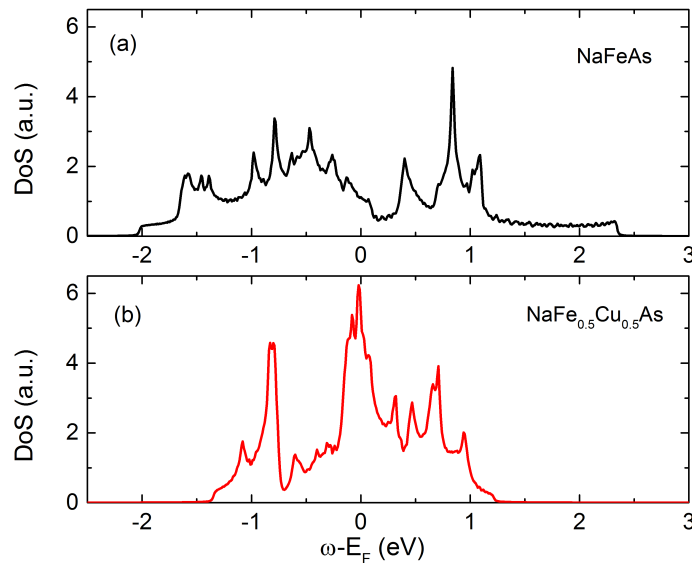
Supplementary Figure 8 |Schematic depiction of the in-plane AF ordering in $\text{NaFe}_{0.5}\text{Cu}_{0.5}\text{As}$ (left panel) used by the electronic structure calculations. Rows of Cu atoms (red) turn out to carry no magnetic moment, whereas spins of Fe atoms (blue) take on the arrangement similar to the parent compound NaFeAs (right panel) with the in-plane ordering wave-vector $Q = (1,0)$ in the orthorhombic notation. The rows of Cu atoms alternate in the c -direction, according to the experimentally determined Ib_4am spacegroup. Note that the spin polarization axis is depicted symbolically and is not representative of the actual spin orientation relative to the crystalline axes.



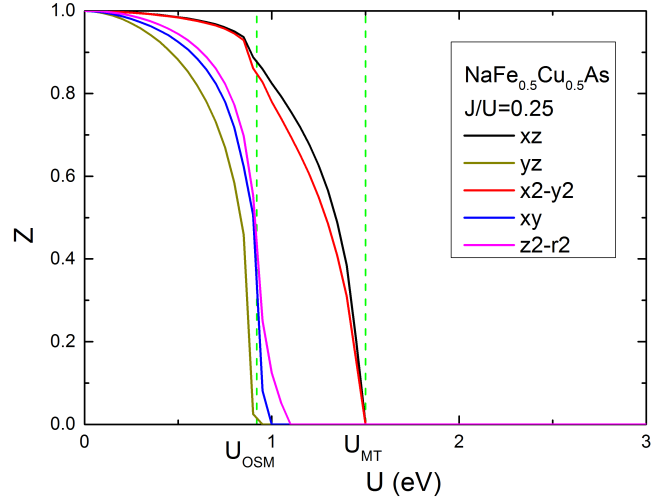
Supplementary Figure 9: Electronic density of states (DOS) calculated with the DFT-GGA method. The paramagnetic phase of (a) parent material NaFeAs, (b) NaFe_{0.5}Cu_{0.5}As. Partial density of states due to d -electrons of Fe and Cu are shown, together with the As p -electron contribution. The zero of energy is chosen to be at the Fermi level, indicated with a vertical dashed line. (c) Attempt to capture the effect of the Coulomb repulsion in paramagnetic NaFe_{0.5}Cu_{0.5}As results in a metallic ground state within the DFT+ U method [see Supplementary Note 4 for details].



Supplementary Figure 10: Electronic density of states in the antiferromagnetically ordered phase of $\text{NaFe}_{0.5}\text{Cu}_{0.5}\text{As}$ calculated with (a) DFT-GGA method, and (b) DFT+U method. Partial contribution to the density of states due to d -electrons of Fe and Cu and p -electrons of As are shown. The insets show the zoomed-in details of the DOS near the Fermi level (denoted by a dashed line).



Supplementary Figure 11: Non-interacting density of states (DoS) of the models for (a) NaFeAs and (b) $\text{NaFe}_{0.5}\text{Cu}_{0.5}\text{As}$, respectively.



Supplementary Figure 12: Calculated orbital-resolved quasiparticle spectral weights of the multiorbital Hubbard model for $\text{NaFe}_{0.5}\text{Cu}_{0.5}\text{As}$. Here, we have taken the electron filling $n=5$ per Fe ion and $J/U=0.25$.

Atom	Site	x	y	z	Occupancy	$U_{\text{iso}}(10^{-2}\text{\AA})$
Na	$8j$	0.17498(52)	0.23423(70)	0	1.0	1.11(18)
As	$8j$	0.89665(27)	0.25595(36)	0	1.0	0.73(15)
Fe1	$4b$	0.5	0	0.25	1.03(13)	0.47(10)
Cu1	$4b$	0.5	0	0.25	-0.03(13)	0.47(10)
Fe2	$4a$	0	0	0.25	0.26(11)	1.00(13)
Cu2	$4a$	0	0	0.25	0.74(11)	1.00(13)

Supplementary Table 1: Structure of $\text{NaFe}_{0.56}\text{Cu}_{0.44}\text{As}$ with Fe-Cu stripe order with the space group $Ibam$ from single crystal neutron diffraction refinement at 250K. The notation used is different from Fig. 1(d) in main text. The fit lattice parameters are $a = 13.85(2)$ Å, $b = c = 5.723(9)$ Å. Twin 1 scale factor 1.821(78), twin 2 scale factor 0.960(59). $R_f = 3.13\%$, $R_g = 4.46\%$, $\chi^2 = 0.794$.

Q_{twin1}	Q_{twin2}	I_{obs}	I_{calc}
1 -1 0	1 0 -1	0.61(6)	0.5970
-1 0 1	-1 1 0	0.35(7)	0.3175
3 0 1	3 1 0	0.31(10)	0.5661
5 1 2	5 2 1	1.82(21)	1.9646
9 2 3	9 3 2	3.56(31)	3.5543
9 3 4	9 4 3	0.70(20)	0.5188
1 1 0	1 0 1	0.66(6)	0.5970
7 2 1	7 1 2	0.38(13)	0.5404
3 3 2	3 2 3	2.85(26)	2.7429
5 4 3	5 3 4	4.92(35)	3.9764
9 4 3	9 3 4	0.74(27)	0.8646
7 5 4	7 4 5	1.07(35)	0.6652
5 3 0	5 0 3	5.07(29)	5.5651
15 3 0	15 0 3	0.92(25)	1.4295
9 4 1	9 1 4	1.27(35)	2.1441
13 4 1	13 1 4	2.03(58)	3.9126
1 5 2	1 2 5	1.39(28)	1.0085
5 5 2	5 2 5	12.75(67)	10.6521
9 5 2	9 2 5	1.34(34)	1.3046
1 6 3	1 3 6	5.95(72)	5.8215
5 6 3	5 3 6	0.96(38)	1.5489
7 5 0	7 0 5	0.62(30)	0.4075

Supplementary Table 2: Measured and calculated super-lattice peak intensities for $\text{NaFe}_{0.56}\text{Cu}_{0.44}\text{As}$ with the space group *Ibam* from single crystal neutron diffraction. Due to twinning measured intensity at (H, K, L) has contributions from (H, K, L) from twin 1 and (H, L, K) from twin 2. Peaks with no measurable intensities are not listed.

Sample/lattice parameter	Atom	Site	x	y	z	Occupancy	U_{iso} (10^{-2}\AA)
$\text{NaFe}_{0.984}\text{Cu}_{0.016}\text{As}$ $a = 3.9546(1)\text{\AA}$ $c = 7.0373(3)\text{\AA}$	Na	2c	0.25	0.25	0.3555(7)	1	1.9(1)
	Fe	2a	0.75	0.25	0	0.984	1.25(4)
	Cu	2a	0.75	0.25	0	0.016	1.25(4)
	As	2c	0.25	0.25	0.7973(4)	1	1.33(6)
$\text{NaFe}_{0.82}\text{Cu}_{0.18}\text{As}$ $a = 3.9985(1)\text{\AA}$ $c = 6.9932(3)\text{\AA}$	Na	2c	0.25	0.25	0.3554(4)	1	1.61(7)
	Fe	2a	0.75	0.25	0	0.82	1.14(4)
	Cu	2a	0.75	0.25	0	0.18	1.14(4)
	As	2c	0.25	0.25	0.7954(2)	1	1.09(5)
$\text{NaFe}_{0.61}\text{Cu}_{0.39}\text{As}$ $a = 4.0353(2)\text{\AA}$ $c = 6.9468(5)\text{\AA}$	Na	2c	0.25	0.25	0.3601(7)	1	1.6(1)
	Fe	2a	0.75	0.25	0	0.61	1.12(7)
	Cu	2a	0.75	0.25	0	0.39	1.12(7)
	As	2c	0.25	0.25	0.7960(3)	1	1.04(7)
$\text{NaFe}_{0.56}\text{Cu}_{0.44}\text{As}$ $a = 4.0472(1)\text{\AA}$ $c = 6.9262(3)\text{\AA}$	Na	2c	0.25	0.25	0.3601(7)	1	1.6(1)
	Fe	2a	0.75	0.25	0	0.61	1.12(7)
	Cu	2a	0.75	0.25	0	0.39	1.12(7)
	As	2c	0.25	0.25	0.7960(3)	1	1.04(7)

Supplementary Table 3: Refinement results from neutron powder diffraction data on $\text{NaFe}_{1-x}\text{Cu}_x\text{As}$. All measurements are taken at 300 K and are fit using $P4/nmm$ space group as super-lattice peaks are too weak to be seen in powder diffraction data. For $\text{NaFe}_{0.984}\text{Cu}_{0.016}\text{As}$, $R_p = 5.08\%$, $wR_p = 6.38\%$ and $\chi^2 = 1.130$. For $\text{NaFe}_{0.82}\text{Cu}_{0.18}\text{As}$, $R_p = 4.20\%$, $wR_p = 5.14\%$ and $\chi^2 = 1.270$. For $\text{NaFe}_{0.61}\text{Cu}_{0.39}\text{As}$, $R_p = 4.11\%$, $wR_p = 5.02\%$ and $\chi^2 = 1.123$. For $\text{NaFe}_{0.56}\text{Cu}_{0.44}\text{As}$, $R_p = 4.79\%$, $wR_p = 5.97\%$, $\chi^2 = 1.098$.

Supplementary Note 1: Fe and Cu ordering in NaFe_{1-x}Cu_xAs as seen in diffraction measurements

The crystal structure of NaFe_{0.56}Cu_{0.44}As obtained from single crystal neutron diffraction refinement is shown in Supplementary Table S1. We collected 120 reflections at Bragg peaks associated with the NaFeAs structure and measured 95 super-lattice peak positions. 22 super-lattice peaks with measurable intensities are identified (Supplementary Table S2), these peaks are refined together with Bragg peaks associated with the NaFeAs structure (not shown). Due to twinning the measured intensity at (H,K,L) have contributions from (H,K,L) from twin 1 and (H,L,K) from twin 2. Population of the twins is roughly 2:1 for this particular sample. Due to formation of Fe-Cu stripes, y positions of Na and As also shift from their high symmetry position 0.25 by δ_{Na} and δ_{As} , respectively.

The crystal structure for NaFe_{0.56}Cu_{0.44}As in Supplementary Table 1 approximates the ideal structure of NaFe_{0.5}Cu_{0.5}As as shown in Figure 1(d), where Fe and Cu order into stripes forming a structural analog of the stripe magnetic order in NaFeAs. This reduces the symmetry of the system to *Ibam* space group. We adopt a unit cell similar to the orthorhombic structural unit cell of NaFeAs throughout the rest of paper as shown in Figure 1(d) unless otherwise stated. Compared to the *Ibam* notation used in Supplementary Table 1, a , b and c in this notation correspond to b , c , and half of a in the *Ibam* notation. In the notation used in Figure 1(d), super-lattice peaks due to Fe-Cu ordering occur at (H,K,L) with $H = 1, 3, 5, \dots$, $K = 0, 2, 4, \dots$ and $L = 0.5, 1.5, 2.5, \dots$. Magnetic peaks in this notation occur at (H,K,L) with $H = 0, 2, 4, \dots$, $K = 1, 3, 5, \dots$ and $L = 0.5, 1.5, 2.5, \dots$ and (H,K,L) with $H = 1, 3, 5, \dots$, $K = 1, 3, 5, \dots$ and $L = 0, 1, 2, \dots$.

To illustrate the effect of Fe-Cu ordering seen in neutron diffraction experiments, calculated neutron powder diffraction profiles for NaFe_{0.5}Cu_{0.5}As with (i) disordered Fe and Cu and $\delta_{\text{As}} = \delta_{\text{Na}} = 0$, (ii) ordered Fe and Cu and $\delta_{\text{As}} = \delta_{\text{Na}} = 0$ and (iii) ordered Fe and Cu with $\delta_{\text{As}} = \delta_{\text{Na}} = -0.01$ are compared in Supplementary Figure 1 assuming $b = c$ (*Ibam* notation). With this assumption, case (i) becomes tetragonal with *P4/nmm* symmetry. In case (ii) where Fe-Cu order into stripes, the only effect is to induce super-lattice peaks without affecting the intensity of nuclear Bragg peaks already present in case (i). For case (iii), introducing non-zero δ_{As} and δ_{Na} , nuclear Bragg peaks already present in case (i) change only slightly.

Given these considerations and for NaFe_{1-x}Cu_xAs with $x < 0.5$ the already weak super-lattice peaks become weaker and broader with decreasing doping [Supplementary Figure 5(f)] we use *P4/nmm* space group appropriate for NaFeAs in the tetragonal state [1] to fit the our room temperature neutron powder diffraction (NPD) data for NaFe_{1-x}Cu_xAs. Doing so the information related to Fe-Cu ordering is neglected but other aspects of the structure can still be reliably obtained. Since the Fe-Cu ordering exists already at room temperature [Figure 2(c)], it will be interesting in future work to see if an order-disorder transition occurs at elevated temperatures where *P4/nmm* symmetry can be recovered with Fe and Cu becoming disordered and $\delta_{\text{As}} = \delta_{\text{Na}} = 0$ corresponding to case (i).

The NPD refinement results for NaFe_{1-x}Cu_xAs with $x = 0.016, 0.18, 0.39$ and 0.44 at room temperature are shown in Supplementary Figures 2(a)-(d) and the refined structural parameters are shown in Supplementary Table 3. Na and As occupancies are assumed to be 1, refinements of their occupancies also yield values close to 1. Given the similar scattering lengths of Fe and Cu, the occupancies of these two elements are set to values determined from ICP. The NPD data at 4K for NaFe_{1-x}Cu_xAs with $x = 0.44$ is shown in Supplementary Figure 2(e). Only one super-lattice/magnetic peak is clearly seen as shown in the inset, so it is not possible to reliably refine δ_{As} and δ_{Na} from NPD data. Instead this data is used to estimate size of the ordered moment, refining the ordered moment for the magnetic structure in Figure 1(d) assuming Fe-Cu ordering we find $1.12(9)\mu_{\text{B}}$ [Supplementary

Figure 2(e)], whereas assuming disordered Fe and Cu we obtain $1.4(1)\mu_B$. (0,0,1), (1,0,1) and (1,1,0) shown in the inset of Supplementary Figure 2(e) are in *Ibam* notation [Supplementary Table 1], corresponding to (0,1,0), (0,1,0.5) and (1,0,0.5) respectively in the notation of Figure 1(d).

Supplementary Note 2: XAS and RIXS measurements on the valence of Cu in NaFe_{0.56}Cu_{0.44}As

XAS for NaFe_{1-x}Cu_xAs ($x = 0.44$) is shown in Supplementary Figure 3(a) for both π and σ polarizations [2], compared with XAS of SrCuO₂ (dashed line) measured with identical experimental configuration. The absorption peak at 930.7 eV in SrCuO₂ due to Cu²⁺ is absent in NaFe_{1-x}Cu_xAs ($x = 0.44$), demonstrating Cu¹⁺ valence in heavily Cu-doped NaFe_{1-x}Cu_xAs samples. Previous results on Cu in different valence states [3] show a chemical shift of ~ 2 eV between the absorption peaks for Cu¹⁺ and Cu²⁺. This agrees with our observation that the sharp absorption peak (931.8 eV) in NaFe_{1-x}Cu_xAs ($x = 0.44$) is higher than the Cu²⁺ absorption peak in SrCuO₂, suggesting that Cu in NaFe_{1-x}Cu_xAs assumes the Cu¹⁺ oxidation state. The two overlapping peaks at ~ 935.5 eV and 936.5 eV are likely due to traces of unreacted elemental Cu. We have further searched for magnetic excitations with resonant inelastic X-ray scattering (RIXS) CuL₃ edge, but did not observe indication for magnetic modes for any of the sampled momentum transfers, typical scans at $Q = (0.23, 0.23)$ are shown in Supplementary Figure 3(b). The absence of magnetic excitations is expected for Cu¹⁺ with a Cu 3d¹⁰ electronic configuration. Thus, both XAS and RIXS results confirm that Cu is in the nonmagnetic Cu¹⁺ state and the elastic magnetic order observed by neutron scattering is entirely due to Fe.

Supplementary Note 3: Additional neutron scattering results

The ordered moment sizes were estimated from normalizing rocking scans of magnetic peaks against a weak nuclear Bragg peak (2, 0, 0) in single crystal elastic neutron scattering measurements. While super-lattice peaks occur at (1, 0, 0.5) and equivalent wave-vectors and magnetic peaks occur at (0, 1, 0.5) and equivalent positions, they overlap in reciprocal space due to twinning. Supplementary Figure 4 shows scans along the $[H, 0, L]/[0, K, L]$ directions at 3.6 K and 300 K for the $x = 0.44$ sample. In Supplementary Figure 5(a), the Q -dependence of magnetic peak intensities are shown, the magnetic intensities are obtained from rocking scans at 3.6 K after correcting for the super-lattice contributions using the ratio of peak intensities at 3.6 K and 300 K shown in Supplementary Figure 4 and the Lorentz factor. In Supplementary Figure 5(b)-(c), the calculated Q dependence of magnetic peak intensities are plotted for spins oriented along a , b and c assuming Fe²⁺ magnetic form factor. Comparing the measured Q -dependence in Supplementary Figure 5(a) and the calculated Q -dependence in Supplementary Figure 5(b)-(c), we conclude that the ordered magnetic moments are oriented predominantly along the a axis.

Supplementary Figure 5(d) shows the wave vector dependence of the super-lattice peaks at 300 K, obtained from scans along the $[H, 0, L]/[0, K, L]$ directions in Supplementary Figure 4. This experimental dependence can be qualitatively described by the structure for NaFe_{0.56}Cu_{0.44}As in Supplementary Table 1, as shown in Supplementary Figure 5(e). For NaFe_{1-x}Cu_xAs with $x = 0.39$, both the magnetic peak [Figure 3(a)] and the super-lattice peak [Supplementary Figure 5(f)] are short-range and have similar widths, suggesting the magnetic signal seen arises from Fe-Cu stripe order.

To conclusively determine the orientation of the ordered magnetic moment, we carried out detailed polarized neutron scattering experiments. Since in our notation magnetic peaks occur at (0, K , L) with $K = 1, 3, 5, \dots$ and $L = 0.5, 1.5, 2.5, \dots$ but not ($H, 0, L$) positions, we only see magnetic signal from $[0, K, L]$ scattering plane. We

define neutron polarization directions along momentum transfer \mathbf{Q} as x , perpendicular to \mathbf{Q} but in the $[0, K, L]$ scattering plane as y and perpendicular to the scattering plane as z as shown in Supplementary Figure6(a). As our neutron scattering samples have twin domains, we cannot distinguish the $(H, 0, L)$ from the $(0, K, L)$ positions in these measurements.

Since SF neutron diffraction is only sensitive to spin components perpendicular to both momentum transfer \mathbf{Q} and neutron polarization direction, one can conclusively determine the spin components along all crystallographic axes M_a , M_b and M_c from the observed magnetic peaks. M_a , M_b and M_c can be obtained via, $\sigma_x^{SF} - \sigma_y^{SF} \propto M_y = \sin^2 \theta M_b + \cos^2 \theta M_c$ and $\sigma_x^{SF} - \sigma_z^{SF} \propto M_z = M_a$, where σ_x^{SF} , σ_y^{SF} and σ_z^{SF} are neutron SF scattering cross sections with polarization directions along x , y and z , respectively, and θ is the angle between momentum transfer \mathbf{Q} and $(0, 1, 0)$. Supplementary Figure 6(b) shows the wave vectors probed in $[0, K, L]$ scattering plane and the corresponding θ . In all cases $M_z = M_a$ while for momentum transfer with small θ , M_y is most sensitive to M_c and for momentum with larger θ , M_y is most sensitive to M_b . Measuring at the momentum transfers shown in Supplementary Figure 6(b), it can be seen in Supplementary Figure 6(c)-(f) that a clear peak can be seen for M_z but no peak is seen for M_y in all cases. These results conclusively show that spins are along the a axis, with negligible spin components along the other two directions, in agreement with our conclusion from unpolarized neutron diffraction results in Supplementary Figure 5(a)-(c).

In Supplementary Figure7(a)-(b), the temperature dependence of magnetic and super-lattice peaks of $\text{NaFe}_{0.56}\text{Cu}_{0.44}\text{As}$ are shown for $\mathbf{Q} = (1,0,0.5)/(0,1,0.5)$ and $\mathbf{Q} = (1,1,0)$ respectively. At both wave-vectors, the SF channel shows magnetic signal with $T_N \sim 200\text{K}$. At $\mathbf{Q} = (1,0,0.5)$, the super-lattice peak appears in the NSF channel and is weakly temperature dependent. At $\mathbf{Q} = (1,1,0)$, there is no signal in the NSF channel below 200K, consistent with this wave-vector being forbidden in the structures of NaFeAs and $\text{NaFe}_{0.5}\text{Cu}_{0.5}\text{As}$ in Figure 1(c) and (d).

Supplementary Note 4: Electronic Structure Calculations for $\text{NaFe}_{0.5}\text{Cu}_{0.5}\text{As}$

Paramagnetic phase:

We first studied the non-magnetic phase of $\text{NaFe}_{0.5}\text{Cu}_{0.5}\text{As}$, using the space group $Ibam$ deduced from the high-resolution TEM and single crystal neutron diffraction measurements [Supplementary Table 1]. The electronic density of states calculated with DFT-GGA method is shown in Supplementary Figure 9(b). The calculations indicate that $\text{NaFe}_{0.5}\text{Cu}_{0.5}\text{As}$ is expected to be a good metal, with the DOS at the Fermi level of 2.5 states per formula unit (f.u.). It is instructive to compare this value to the DOS in the parent compound NaFeAs [Supplementary Figure 9(a)], which is actually lower at ~ 2.0 states per f.u. This is understood because in NaFeAs , the Fermi level lies near a trough of the DOS, whereas in $\text{NaFe}_{0.5}\text{Cu}_{0.5}\text{As}$, it sits of the shoulder of the Fe d -state peak. This is also consistent with the fact that the Fe d -electron bandwidth is narrower than in NaFeAs , resulting in a larger DOS.

At first sight, the theoretical finding of the metallic behavior is puzzling, given the experimental observation of the insulating nature of $\text{NaFe}_{0.56}\text{Cu}_{0.44}\text{As}$. Conceivably, this may be an indication of the failure of the *ab initio* theory, since strong electron correlations are notoriously difficult to capture with DFT. To estimate the effect of the Coulomb repulsion U , we have performed a DFT+ U calculation [4] on $\text{NaFe}_{0.5}\text{Cu}_{0.5}\text{As}$ using the interaction strength $U = 3.15$ eV and Hund's coupling $J = 0.4$ eV calculated in Ref. [5]. Curiously, although Coulomb repulsion does reduce the DOS by creating a pseudogap like feature at the Fermi level, it still predicts $\text{NaFe}_{0.5}\text{Cu}_{0.5}\text{As}$ to be a metal (DOS(E_F) ~ 2.1 states/f.u.) rather than an insulator in the paramagnetic state, as shown in Supplementary Figure 9(c). This is in stark contrast to the experimentally measured resistivity, which

exhibits insulating behavior even in the paramagnetic phase, above the AF ordering temperature in $\text{NaFe}_{0.5}\text{Cu}_{0.5}\text{As}$ [see Figure 2(f) in the main text]. Clearly, strong electron correlations are present that are not captured properly by the DFT or DFT+ U calculations in the paramagnetic phase.

Antiferromagnetic phase:

We have also calculated the AF configuration of $\text{NaFe}_{0.5}\text{Cu}_{0.5}\text{As}$, which turns out to be more stable than the paramagnetic state by 0.28 eV/f.u. in our DFT-GGA calculations. We note that the antiferromagnetic order lowers the symmetry of the paramagnetic $Ibam$ space group down to its subgroup $I222$. The Fe magnetic moments order in the (ab)-plane according to the experimentally observed $\mathbf{Q} = (1,0)$ wave-vector, as depicted schematically in the left panel of Supplementary Figure 8. The value of the ordered moment is predicted by DFT to be $2.77 \mu_B$ on Fe site, larger than the experimentally measured ordered moment of $\sim 1.4 \mu_B$ per Fe. We find that the Cu moment is essentially zero ($\sim 0.02 \mu_B$), consistent with the full shell Cu^{1+} (d^{10}) configuration inferred from the experiments. Calculations within the DFT-GGA formalism show that the electronic density of states at the Fermi level is severely suppressed in the AF state, as shown in Supplementary Figure 10(a). Including the effect of the Coulomb repulsion using the DFT+ U approach opens up a spectral gap of about 0.1 eV at the Fermi level, resulting in the true *insulating* state. The DFT+ U also predicts Cu ions to be non-magnetic, while stabilizing an even higher ordered moment on Fe sites ($3.29 \mu_B$ per Fe).

It is instructive to compare the *ab initio* AF calculations with the experiment. In DFT and DFT+ U calculations, the entire ordered moment comes from Fe site, while Cu ions are non-magnetic. While this is consistent with our experimental results, the predicted moment is much larger ($2.77 \mu_B$ in GGA) than the experimentally measured value of $\sim 1.4 \mu_B$.

In conclusion, theoretical electronic structure calculations based on DFT and DFT+ U indicate that the value of Coulomb repulsion is not large enough by itself to result in the paramagnetic Mott insulating state in $\text{NaFe}_{0.5}\text{Cu}_{0.5}\text{As}$, which appears to contradict the observed insulating behavior of resistivity [Fig. 1(f) in the main text]. Allowing the possibility of an AF ordering amplifies the effect of Coulomb interaction, resulting in an insulating magnetic ground state. However, the theory predicts the average value of the ordered moment per Fe site too large compared with the experimental value from neutron diffraction. This deficiency of DFT in exaggerating the ordered Fe moment is well documented in other materials in the iron pnictide family [5, 6]. The electronic structure calculations do capture correctly an enhanced propensity to AF ordering when compared to the parent compound NaFeAs , which has a very small ordered moment $\sim 0.1 \mu_B/\text{Fe}$ [1]. This is consistent with the electronic correlations becoming stronger upon Cu doping.

Supplementary Note 5: Effects of electron correlations

An important consequence of the large local potential difference between Cu and Fe is the kinetic blocking mechanism: the hopping process between Cu and Fe ions are substantially reduced in $\text{NaFe}_{0.5}\text{Cu}_{0.5}\text{As}$ compared to that between Fe-Fe ions in NaFeAs . Within our approximation, such a kinetic blocking mechanism completely suppresses the inter Fe-Cu and intra Cu-Cu hoppings. This effectively reduces the kinetic energy. As for the hopping integrals between Fe-Fe, we adopt the same tight-binding parameters as in NaFeAs . With this setup, we have calculated the density of states in the non-interacting limit of models for NaFeAs and $\text{NaFe}_{0.5}\text{Cu}_{0.5}\text{As}$, respectively. As shown in Supplementary Figure 11, the overall bandwidth of the $\text{NaFe}_{0.5}\text{Cu}_{0.5}\text{As}$ is reduced from the one of NaFeAs by a factor about 41%. As we will discuss later in this section, this kinetic energy reduction is crucial to stabilizing a Mott insulating state in $\text{NaFe}_{0.5}\text{Cu}_{0.5}\text{As}$.

For NaFeAs, a metal-to-Mott-insulator transition takes place when U exceeds about 5 eV. For sufficiently large J/U , this transition involves a third intermediate orbital-selective Mott phase (OSMP), where the Fe $3d_{xy}$ orbital is Mott localized with zero quasiparticle spectral weight, while all other $3d$ orbitals are still itinerant. Note that similar OSMP has been found in a model for $K_xFe_{2-y}Se_2$ system [7]. In the metallic phase, there is a crossover from a weakly coupled metallic state to a strongly coupled one, at which the quasiparticle spectral weights drop rapidly. In the strongly coupled metallic state, the quasiparticle spectral weight shows strong orbital selectivity. Such a crossover is a quite general feature of the models for both iron pnictides and iron chalcogenides [7,8].

To estimate the strength of electron correlations in the NaFeAs system, we compare the bandwidth renormalization factor calculated from our theoretical model to the one obtained in ARPES experiments. In Ref. [9], an overall bandwidth renormalization factor of 4 has been reported. Here we estimate the J and U values of the system by requiring the theoretically calculated renormalization factor $1/Z_\alpha$ for each orbital α between 2 to 6. We then assume that the J and U values in the NaFeAs and NaFe_{0.5}Cu_{0.5}As systems are comparable. These estimated parameter values form a “physical” parameter regime in the phase diagram, which is shown as the shaded regime in Fig.4(c) of the main text.

By treating the Cu ions as vacancies, we obtain the phase diagram of the model for NaFe_{0.5}Cu_{0.5}As, as shown in Fig.4(c) of the main text. The evolution of quasiparticle spectral weights with U at $J/U=0.25$ for NaFe_{0.5}Cu_{0.5}As is shown in Supplementary Figure 12. There are three phases, a metallic one, an OSMP, and a Mott insulator. Compared to the case of NaFeAs, the critical U for the Mott transition (U_{MT}) at any given J/U value is substantially reduced. This reduction of U_{MT} can be readily understood. As mentioned above, the local potential difference between the Cu and Fe sites leads to kinetic blocking, which reduces the kinetic energy. This effect is augmented by the valence of Fe being Fe³⁺ (with $n = 5$), which also originates from the local potential difference between the Cu and Fe sites. The reduction of U_{MT} in the model for NaFe_{0.5}Cu_{0.5}As already pushes the “physical” parameter regime to lie inside the Mott insulating part of the phase diagram. Our theoretical result is consistent with our experimental one, which indicates that NaFe_{0.5}Cu_{0.5}As is a Mott insulator.

Supplementary References

- [1] Li, S. *et al.* Structural and magnetic phase transitions in Na_{1-δ}FeAs, *Phys. Rev. B* **80**, 020504(R) (2009).
- [2] Zhou, K.-J. *et al.* Persistent high-energy spin excitations in iron-pnictide superconductors, *Nat. Commun.* **4**, 1470 (2013).
- [3] Jiang, P. *et al.* Experimental and theoretical investigation of the electronic structure of Cu₂O and CuO thin films on Cu(110) using x-ray photoelectron and absorption spectroscopy, *J. Chem. Phys.* **138**, 024804 (2013)
- [4] Anisimov, V. I., Zaanen, J. & Andersen, O. K. Band theory and Mott insulators: Hubbard U instead of Stoner I , *Phys. Rev. B* **44**, 943-954 (1991).
- [5] T. Miyake, K. Nakamura, R. Arita, & M. Imada, *J. Phys. Soc. Jpn.* **79**, 044705 (2010).
- [6] Mazin, I. I., Johannes, M. D., Boeri, L., Koepnick, K. & Singh, D. J. Problems with reconciling density functional theory calculations with experiment in ferropnictides, *Phys. Rev. B* **78**, 085104 (2008).
- [7] Yu, R. & Si, Q. Orbital-Selective Mott Phase in Multiorbital Models for Alkaline Iron Selenides $K_{1-x}Fe_{2-y}Se_2$, *Phys. Rev. Lett.* **110**, 146402 (2013).
- [8] Yu, R. & Si, Q. $U(1)$ slave-spin theory and its application to Mott transition in a multiorbital model for iron pnictides, *Phys. Rev. B* **86**, 085104 (2012).
- [9] Yi, M. *et al.* Electronic reconstruction through the structural and magnetic transitions in detwinned NaFeAs, *New J. Phys.* **14**, 073019 (2012).

Editorial Note: this manuscript has been previously reviewed at another journal that is not operating a transparent peer review scheme. This document only contains reviewer comments and rebuttal letters for versions considered at Nature Communications.

Reviewers' comments:

Reviewer #1 (Remarks to the Author):

The authors have submitted a new version of the manuscript which address the criticisms raised by myself and the other Referees. The authors in particular have addressed my main points (1) and (2) of the previous report.

The new version of the manuscript is certainly much clearer and several potentially misleading aspects have been eliminated. Also the discussion about the theoretical literature is more faithful and complete.

In particular the authors acknowledge the ambiguity of the original formulation, where the Mott insulator studied in this manuscript was claimed to be "near" the superconducting state. The authors now clearly state that the key point of the manuscript is to report a smooth connection between the superconductor and the Mott insulator which is realized by substituting Fe with Cu.

I am perfectly fine with this clarification and I agree with the authors that this is the first case where a Mott state is continuously connected with a superconducting state in the iron-superconductor family (although two places can be smoothly connected, yet very far). I am not equally sure that the new version of the title is actually much better than than the original one. In my mind, the expression "entwined" is quite evocative, but it does not convey a clear physical message. I would suggest the authors to use the expression "smoothly connected" also in the title.

Turning from semantics to physics, I think that the revised manuscript presents more correctly what happens when Fe is replaced by Cu. Based on the experimental information that Cu is in a d10 configuration for $x=0.5$ and on the theoretical calculations for the same endpoint compound, it appears clear that Cu-doping leads to at least two main effects which favor a Mott transition: (1) a change of the effective charge on Fe orbitals from 6 to 5 and (2) a reduction of kinetic energy due to the vacancies. While the two points are reasonably well stressed in the conclusions, in the introductory part the authors still omit the important fact that the iron sites are effectively hole doped (Sentence: "which show that a Cu-site blockage of the kinetic motion of the Fe 3d electrons reduces the electron bandwidth and thus enhances the effect of electron correlations, pushing the system towards Mott localization"). The doping effect should be clearly mentioned also in this section, also citing the papers that put emphasis on the role of the d5 configuration, namely Refs. 10 and 11 and to a lesser extent Ref. 9.

Once the readership is clearly informed that these are the two main effects which both contribute to drive the Mott transition, it can decide if one of the two effects is more important or if they are both necessary. Of course the authors can add their arguments for one of the other mechanism, but this should be separated from the presentation of the actual results.

In this way it is also easier to rationalize in which sense we can consider the $x=0.5$ material close (or far) to the superconductor with $x=0$. If we refer to a generic diagram such as Fig. 7 of Ref. 37, NaFeAs is in the blue region at $N=6$. Cu substitution drives us to some point on the $N=5$ axis with a larger

value of U/W , deeply in the Mott state.

I also find quite unfair to quote Ref. 37 for the “general theoretical investigation of a Mott insulating state in an overall phase diagram”. The diagram of Ref. 37 is a schematic summary of many previous investigations including very basic physical facts and less obvious aspects related to the Hund’s coupling. I think that the above sentence should quote all the above theoretical works where the possible role of both the $n=6$ and $n=5$ Mott transitions has been discussed, including 9-11.

I am satisfied by the other replies by the authors.

Finally, a very minor point. When the authors conclude that the role of strong correlations can be unifying framework of several superconductors, they might add also the alkali-doped fullerides, where the role of strong correlations seems nowadays established [See for example, the recent paper by Nomura et al. *Science Advances* 1, e1500568 (2015)]

In conclusion, I think that the present manuscript can be published in *Nature Communications* once the authors take into account my last comments.

Reviewer #2 (Remarks to the Author):

I have carefully read the revised manuscript and the authors’ response. I appreciate the authors’ performing new x-ray experiments to determine the valence state of Cu. I agree with the authors’ assessment that their set of experimental measurements provides strong evidence for a Mott insulating state for samples with concentrations near $x=0.5$.

The main issues, however, are about the novelty of this finding and its impact to the understanding of superconductivity in iron-based compounds. On the latter issue, which in my view is the most critical one, the several changes made by the authors are not only unconvincing, but they seem to actually support the opposite point of view, namely that this Mott insulating phase seems nearly inconsequential to the superconducting state. The authors now claim that the Mott insulator near $x=0.5$ is not “near”, but rather “entwined” and “smoothly connected” with the superconducting state at $x=0.016$. To support this claim, they now plot in Fig. 1g the “ordered magnetic moment” as function of x , instead of the Neel transition temperature (which is restricted to the region near $x=0.5$). The first problem is that, since there are no data points for concentrations below $x=0.18$, I do not understand how the authors can justify that the “ordered magnetic moment” line shown in Fig. 1g ends precisely at the end of the superconducting dome at much smaller doping levels, $x=0.04$. The second – and most important – issue is that this plot contradicts Fig. 3c: as the authors state in the main text, there is no long-range magnetic order for $x<0.44$, as shown by both resistivity and neutron scattering data. Therefore, there is no meaning in assigning an “ordered magnetic moment” in that region of the phase diagram, where at best one has only short-ranged fluctuations with correlation lengths of a few lattice parameters, as shown in Fig. 3c. Finally, as the authors discuss in the paper, the Mott insulating state seems to be favored by the specific Cu concentration of $x=0.5$, which causes real space Fe/Cu order and changes the valence of Fe to $3d^5$. In this case, it is very hard to conceive a scenario in which this peculiar Mott state is “smoothly connected” to the $x=0$ compound.

On the issue of novelty, although it is true that the STM studies in Ref. [16] could not unambiguously determine the Mott insulating nature of this phase, they did provide solid indirect evidence in favor of this state. Of course, the current work goes well beyond Ref. [16] by extending the phase diagram to $x=0.44$ and by combining a series of thermodynamic measurements that exclude other possible sources for the insulating state. Nevertheless, in my opinion, this does not provide a major

advancement, in view of the issues raised above. With appropriate and substantial revisions, the paper might be suitable for publication in a more specialized journal.

Reviewer #3 (Remarks to the Author):

I have read the revised version of the manuscript and the authors' rebuttal. My summary of the key results and other comments on the quality of the data, presentation and appropriateness of the references remain unchanged. The authors have made a serious effort to address the referees' concerns, including performing further experiments. In particular the authors show convincingly by single crystal neutron diffraction that a substantially fraction of the sample has Fe/Cu order, which strengthens the conclusion that the 50% doped sample is a Mott insulator. In my opinion the manuscript is now suitable for publication in Nature Communications.

Reviewer #4 (Remarks to the Author):

In this manuscript, the authors successfully observe an AF insulating state in heavily Cu-doped $\text{NaFe}_{1-x}\text{Cu}_x\text{As}$ material. Moreover, the authors claim that the possibility of insulating state due to Anderson localization could be excluded due to the confirmed ordering arrangement of Cu and Fe atoms in the FeAs plane. From additional XAS and RIXS experiments, the authors also conclusively confirm the $3d^{10}$ electronic configuration of Cu in $x=0.50$ material, which strongly support their previous assertion of $3d^5$ Fe configuration is in fact correct. Based on these facts, I think that the conclusion on Mott insulating phase in $x=0.50$ material is solid. Based on this finding, the authors also obtained a new phase diagram for Cu-doped NaFeAs as shown in Fig.1(g) which suggests a close connection between Mott physics and superconductivity in this material. The main controversial point between the authors and other referees for this issue is whether the Mott insulator is close enough to NaFeAs based superconductors to be relevant to superconductivity. In my opinion, Mott physics is unambiguously important for superconductivity in iron-based superconductor. The key point is to clarify how Mott physics affects superconductivity here. In present work, the authors compare this material to electron-doped cuprates. Based on the multi-orbital theoretical consideration, the average electron doping level on each orbital here is believed to be less than 20%, comparable with electron-doped cuprates. I think this consideration is reasonable. Moreover, the recent ARPES experiment confirmed the Mott insulating phase and proves that the conduction band is of Fe $3d$ -like character for heavily Cu-doped $\text{NaFe}_{1-x}\text{Cu}_x\text{As}$ (arXiv:1607.00770). Therefore, the main conclusion in present work is acceptable. In addition, the authors have made a very good reply for all comments raised by all referees. I think the present manuscript is worth to be published in Nature Communications.

REVIEWERS' COMMENTS:

Reviewer #1 (Remarks to the Author):

The authors have satisfactorily replied to the remaining points that I raised in my report. In particular

1) I appreciate the change in the title, which I think will be beneficial for the impact of the paper.

2) I think that the discussion of the previous literature about the role of Mott physics in iron-based superconductors has been improved.

3) I agree with the authors that the experimental reference on the role of Mott physics in Cs₃C₆₀ is more appropriate than the theory paper I mentioned

Incidentally, I think the authors replied satisfactorily also to the other Referee.

The revised manuscript can be published in Nature Communications in the present form.

Response to referee 1

“The authors have submitted a new version of the manuscript which address the criticisms raised by myself and the other Referees. The authors in particular have addressed my main points (1) and (2) of the previous report.

The new version of the manuscript is certainly much clearer and several potentially misleading aspects have been eliminated. Also the discussion about the theoretical literature is more faithful and complete.

In particular the authors acknowledge the ambiguity of the original formulation, where the Mott insulator studied in this manuscript was claimed to be “near” the superconducting state. The authors

now clearly state that the key point of the manuscript is to report a smooth connection between the superconductor and the Mott insulator which is realized by substituting Fe with Cu.”

We appreciate these positive comments from the referee.

“I am perfectly fine with this clarification and I agree with the authors that this is the first case where a Mott state is continuously connected with a superconducting state in the iron-superconductor family (although two places can be smoothly connected, yet very far). I am not equally sure that the new version of the title is actually much better than than the original one. In my mind, the expression “entwined” is quite evocative, but it does not convey a clear physical message. I would suggest the authors to use the expression “smoothly connected” also in the title.”

We have followed the suggestion of the referee and replaced the term ‘entwined with’ by ‘continuously connected to’ in the title of our manuscript.

“Turning from semantics to physics, I think that the revised manuscript presents more correctly what happens when Fe is replaced by Cu. Based on the experimental information that Cu is in a $d10$ configuration for $x=0.5$ and on the theoretical calculations for the same endpoint compound, it appears clear that Cu-doping leads to at least two main effects which favor a Mott transition: (1) a change of the effective charge on Fe orbitals from 6 to 5 and (2) a reduction of kinetic energy due to the vacancies. While the two points are reasonably well stressed in the conclusions, in the introductory part the authors still omit the important fact that the iron sites are effectively hole doped (Sentence: “which show that a Cu-site blockage of the kinetic motion of the Fe 3d electrons reduces the electron bandwidth and thus enhances the effect of electron correlations, pushing the system towards Mott localization”). The doping effect should be clearly mentioned also in this section, also citing the papers that put emphasis on the role of the $d5$ configuration, namely Refs. 10 and 11 and to a lesser extent Ref. 9.

Once the readership is clearly informed that these are the two main effects which both contribute to drive the Mott transition, it can decide if one of the two effects is more important or if they are both necessary. Of course the authors can add their arguments for one of the other mechanism, but this should be separated from the presentation of the actual results.”

In this way it is also easier to rationalize in which sense we can consider the $x=0.5$ material close (or far) to the superconductor with $x=0$. If we refer to a generic diagram such as Fig. 7 of Ref. 37, NaFeAs is in the blue region at $N=6$. Cu substitution drives us to some point on the $N=5$ axis with a larger value of U/W , deeply in the Mott state.”

We thank the referee for these additional comments. In fact, the substance of these remarks is the same as what we said in our previous reply, which we repeat here for convenience: “Having said the above, we wish to clarify the theoretical meaning of the Mott insulating phase in the overall phase diagram. It is well known that proximity to a Mott insulator can be realized in two kinds of ways: by tuning kinetic energy (in the sense that the Referee referred to) or by tuning electron filling. In a multiband system like

here, this phase diagram is even richer because $N=5,6,7$ etc. are all commensurate fillings that harbor the Mott insulating state. The corresponding phase diagram, taking into account the crystal-level splittings, was outlined in R. Yu, Zhu and Si, *Current Opinion in Solid State and Materials Science* 17, 65 (2013), which is now cited as Ref. 37; see Fig. 7 of that reference (or Fig. 4 of F. Eilers et al, arXiv:1510.01857, in press at PRL). The key point to emphasize is that, with a crystal level splitting and orbital selectivity, both $N=5$ and 6 can have orbitals at half-filling giving rise to a Mott insulator. This type of theoretical framework goes back to the earlier studies of some of the present theory co-authors at the beginning of the iron-based-superconductor field. The important work of Ishida and Liebsch, Misawa et al. and de 'Medici et al are done in a similar framework, and citing these references are certainly appropriate; we have added them as Refs. 9-11 in the revised manuscript. In our present work, we have theoretically shown that taking into account the Cu-blockage effect in a similar theoretical framework provides the understanding for the origin of the Mott insulating state experimentally discovered here. We feel that this new theoretical understanding is one of the important accomplishments of the present work and, at the same time, falls within the theoretical framework of an overall phase diagram: with one axis labeling (interaction/kinetic energy) tuning, and the other axis labeling electron filling tuning (which, in our case, spans between $N=6$ and $N=5$).” The important point is that, starting from the very first work of Si and Abrahams, proximity to Mott has always been recognized in the multi-band context and involves both bandwidth and doping tunings. Still, the referee is correct, and that Refs. 9-11 deserve to be cited in the same context.

In our previous revision, we have modified the concluding discussion in this spirit. The referee is now satisfied with this revised version of the concluding discussion, stating that “the two points are reasonably well stressed in the conclusions”.

Here, the referee is reminding us that the one sentence in the introduction part should also be rephrased into the same form. We have followed the advice of the referee and revised the sentence in the introduction so that the referencing is done in the same way as in the conclusion, including to Refs. 9-11.

“I also find quite unfair to quote Ref. 37 for the “general theoretical investigation of a Mott insulating state in an overall phase diagram”. The diagram of Ref. 37 is a schematic summary of many previous investigations including very basic physical facts and less obvious aspects related to the Hund’s coupling. I think that the above sentence should quote all the above theoretical works where the possible role of both the $n=6$ and $n=5$ Mott transitions has been discussed, including 9-11.

We again thank the referee for the comment. The reason that Ref. 37 (now Ref. 38) is used to refer to the general theoretical investigation of a Mott insulating state in an overall phase diagram is precisely because it summarized all the earlier works (including Si and Abrahams, Yu and Si etc..) in addition to the more recent studies. As already mentioned, proximity to Mott always means proximity via BOTH bandwidth tuning and doping tuning, and this predated Refs. 9-11. Nonetheless, Refs. 9-11 do represent important contributions in this overall context and they are indeed included in the citations of the same sentence.

I am satisfied by the other replies by the authors.”

We thank the referee once again for the positive comments regarding our revision.

“Finally, a very minor point. When the authors conclude that the role of strong correlations can be unifying framework of several superconductors, they might add also the alkali-doped fullerides, where the role of strong correlations seems nowadays established [See for example, the recent paper by Nomura et al. Science Advances 1, e1500568 (2015)]”

We thank for the referee for suggesting alkali-doped fullerides to be included in the concluding discussion. To conform to the broad nature of this concluding sentence, we have chosen to refer to the first experimental paper demonstrating the Mott insulating state in the overall phase diagram of this class of superconductors (the new Ref. 40).

“In conclusion, I think that the present manuscript can be published in Nature Communications once the authors take into account my last comments.”

We have addressed all the comments of the referee in our revised manuscript. We thank the referee for his/her recommendation for publication of our work in Nature Communications.

Response to referee 2

“I have carefully read the revised manuscript and the authors’ response. I appreciate the authors’ performing new x-ray experiments to determine the valence state of Cu. I agree with the authors’ assessment that their set of experimental measurements provides strong evidence for a Mott insulating state for samples with concentrations near $x=0.5$.”

We thank the referee for appreciating our efforts and agreeing with us that our experiments establish the samples with concentrations near $x=0.5$ to be a Mott insulating state.

“The main issues, however, are about the novelty of this finding and its impact to the understanding of superconductivity in iron-based compounds. On the latter issue, which in my view is the most critical one, the several changes made by the authors are not only unconvincing, but they seem to actually support the opposite point of view, namely that this Mott insulating phase seems nearly inconsequential to the superconducting state. The authors now claim that the Mott insulator near $x=0.5$ is not “near”, but rather “entwined” and “smoothly connected” with the superconducting state at $x=0.016$. To support this claim, they now plot in Fig. 1g the “ordered magnetic moment” as function of x , instead of the Neel transition temperature (which is restricted to the region near $x=0.5$). The first problem is that, since there are no data points for concentrations below $x=0.18$, I do not understand how the authors can justify that the “ordered magnetic moment” line shown in Fig. 1g ends precisely at the end of the superconducting dome at much smaller doping levels, $x=0.04$.”

With regards to the criticism that we have no data for samples below $x=0.18$ and therefore cannot justify the line of ordered moment terminating at the end of the SC dome, we would like to clarify that (1) the main conclusions of our paper do not rely on the line terminating precisely at the edge of SC dome, and (2) the fact that it does is a result of extrapolating the trend seen from the samples we measured. We agree with the referee that it may be misleading to show the line ending precisely at the edge of SC dome and have therefore removed the line for $x<0.18$.

“The second – and most important – issue is that this plot contradicts Fig. 3c: as the authors state in the main text, there is no long-range magnetic order for $x<0.44$, as shown by both resistivity and neutron scattering data. Therefore, there is no meaning in assigning an “ordered magnetic moment” in that region of the phase diagram, where at best one has only short-ranged fluctuations with correlation lengths of a few lattice parameters, as shown in Fig. 3c. Finally, as the authors discuss in the paper, the Mott insulating state seems to be favored by the specific Cu concentration of $x=0.5$, which causes real space Fe/Cu order and changes the valence of Fe to $3d^5$. In this case, it is very hard to conceive a scenario in which this peculiar Mott state is “smoothly connected” to the $x=0$ compound.”

The referee criticizes the use of ‘ordered moment’ given that the magnetic order is short ranged. We disagree with the referee because for short-ranged such as glassy magnetic order, the ordered moment is still a well-defined quantity. Indeed, for x sufficiently below 0.5, the system is influenced by disorder, and therefore the spatial order is glassy. Nonetheless, in our DIFFRACTION experiment (which, of course, is a quasi-elastic probe), the measured moment is still (quasi-)static. A scenario of how the real-space Fe/Cu is smoothly connected to a state without Cu is simply that with decreasing Cu concentration, the Fe/Cu ordering becomes more and more short-ranged, which is supported by our data (Supplementary Figure 5). Thus, our experiments show that the Mott state is indeed smoothly connected to the superconducting compound near $x=0$. We also wish to remind the referee that our theoretical calculations presented in the main text and in the supplementary material, provide a natural way to smoothly connect the systems near $x=0.5$ with those near $x=0$, through a trajectory in an overall phase diagram that spans both the bandwidth-tuning and doping-tuning axes.

“On the issue of novelty, although it is true that the STM studies in Ref. [16] could not unambiguously determine the Mott insulating nature of this phase, they did provide solid indirect evidence in favor of this state. Of course, the current work goes well beyond Ref. [16] by extending the phase diagram to $x=0.44$ and by combining a series of thermodynamic measurements that exclude other possible sources for the insulating state. Nevertheless, in my opinion, this does not provide a major advancement, in view of the issues raised above. With appropriate and substantial revisions, the paper might be suitable for publication in a more specialized journal.”

We thank the referee for acknowledging that our work goes well beyond Ref. [16]. As agreed by the other three referees, we believe our work presents several important advances: (1) the elucidation of the origin of the insulating state seen in Ref. [16], especially through the new study in the doping regime close to $x=0.5$, (2) the presence of magnetic ordering which, combining with the transport and other measurements both below and above the Neel temperature, allow an unambiguous identification of the

Mott nature of the insulating state, (3) an understanding from both experimental and theoretical perspectives why such a Mott insulating state is stabilized in $\text{NaFe}_{1-x}\text{Cu}_x\text{As}$, and (4) the experimental evidence for – and the theoretical understanding of – the smooth connection between the Mott insulating state and the superconducting regime.

Response to Reviewer #1:

“The authors have satisfactorily replied to the remaining points that I raised in my report. In particular

1) I appreciate the change in the title, which I think will be beneficial for the impact of the paper.

2) I think that the discussion of the previous literature about the role of Mott physics in iron-based superconductors has been improved.

3) I agree with the authors that the experimental reference on the role of Mott physics in Cs₃C₆₀ is more appropriate than the theory paper I mentioned

Incidentally, I think the authors replied satisfactorily also to the other Referee.

The revised manuscript can be published in Nature Communications in the present form.”

We thank the referee for acknowledging that our revised manuscript satisfactorily addressed the concerns raised in his/her previous report and those raised by the other referees, as well as for recommending the publication of our manuscript in the present form.